Fire Behaviour Of Composite Slabs With Steel Deck And Mineral Wool

Israel Mateus Melo Oliveira

Dissertation submitted to the School of Technology and Management from the Polytechnic Institute of Bragança in partial fulfillment of the requirements for the Master Degree in Construction Engineering, within the scope of the Double Degree Program with the Federal Centre for Technological Education of Minas Gerais.

Work carried out under the supervision of:

Prof. Paulo Piloto
Prof. Carlos Balsa
Prof. Luciana Alvarenga

This dissertation does not include the comments and suggestions made by the examination committee.

Bragança, May 2025.

Fire Behaviour Of Composite Slabs With Steel Deck And Mineral Wool

Israel Mateus Melo Oliveira

Dissertation submitted to the School of Technology and Management of the Polytechnic Institute of Bragança in partial fulfillment of the requirements for the Master Degree in Construction Engineering, within the scope of the Double Degree Program with the Federal Centre for Technological Education of Minas Gerais.

Work carried out under the supervision of:

Prof. Paulo Piloto
Prof. Carlos Balsa
Prof. Luciana Alvarenga

Bragança, May 2025.

- **RESUMO**

Este trabalho investiga o comportamento térmico de lajes mistas com chapa de aço colaborante (*steel deck*) submetidas a situação de incêndio, com foco na influência da temperatura sobre o momento fletor positivo. A pesquisa tem como principal objetivo desenvolver uma fórmula simplificada que permita estimar, com precisão, a temperatura média nos elementos que compõem a seção transversal da laje – como o perfil metálico e a armadura, considerando a inexistência de diretrizes normativas que tratem diretamente desse aspecto para estruturas mistas. A avaliação precisa dessas temperaturas é essencial para possibilitar as análises de resistência à flexão em situação de incêndio, uma vez que a degradação térmica dos materiais altera significativamente a capacidade resistente da laje. A metodologia adotada fundamentou-se em simulações térmicas tridimensionais conduzidas no software ANSYS, as quais foram validadas com base em dados experimentais da literatura. A validação demonstrou boa concordância entre os modelos numéricos e os resultados de referência, com erros médios quadráticos (RMSE) aceitáveis para os diferentes pontos analisados. Em seguida, foram realizados 72 estudos paramétricos, nos quais se variaram a espessura do concreto, a espessura da lã de rocha, o diâmetro da armadura e o tempo de exposição ao fogo. A partir desses resultados, foi desenvolvida uma equação linear ajustada por regressão, capaz de prever a temperatura média nos componentes com elevada precisão. Comparada aos dados obtidos no ANSYS, a fórmula proposta apresentou RMSE inferior a 5% em todos os casos analisados, evidenciando sua eficácia como ferramenta auxiliar no dimensionamento térmico de lajes mistas em situação de incêndio.

Palavras-chave: Lajes mistas; comportamento ao fogo; modelagem térmica; fórmula simplificada.

- **ABSTRACT**

This study investigates the thermal behaviour of composite slabs with steel deck under fire conditions, focusing on the influence of temperature on the positive bending moment (sagging moment). The main objective is to develop a simplified formula capable of accurately estimating the average temperature in the structural components of the slab – such as the steel profile and reinforcement, considering the absence of specific normative guidelines for this aspect in composite structures. Accurately assessing these temperatures is essential for supporting the calculation of the flexural resistance under fire exposure, since the thermal degradation of materials significantly affects the load-bearing capacity of the slab. The adopted methodology was based on three-dimensional thermal simulations using ANSYS software, which were validated against experimental data available in the literature. The validation showed good agreement between the numerical models and the reference results, with acceptable root mean square errors (RMSE) for the different evaluated points. Subsequently, 72 parametric studies were carried out, varying the thickness of the concrete, the thickness of the mineral wool, the diameter of the reinforcement bars, and the fire exposure time. From these results, a linear regression-based equation was developed to predict the average temperature in each component with high accuracy. When compared to the ANSYS simulation data, the proposed formula achieved RMSE values below 5% in all cases, demonstrating its effectiveness as a supporting tool for thermal design of composite slabs under fire conditions.

Keywords: Composite slabs; fire behaviour; thermal modelling; simplified formula.

TABLE OF CONTENTS

- **LIST OF FIGURES**

- **LIST OF TABLES**

1. INTRODUCTION

Over the decades, the progress of structural engineering has been driven by the relentless pursuit of innovative solutions to enhance the efficiency and safety of structures. Within this progress, a profound understanding of the thermal effects on composite structures has become a crucial area of interest.

Composite structures subjected to fire refer to construction systems that combine different materials, typically steel and concrete, to create structural elements that are more efficient in terms of strength and thermal performance. These structures are designed to face fire conditions with greater strength and stability than structures composed of a single material.

During a fire, composite structures face significant challenges due to the distinct thermal characteristics of their components. For instance, steel is an excellent heat conductor and may experience a high reduction in strength at high temperatures, while concrete, with higher thermal resistance, can suffer damage due to thermal expansion.

Composite structures are often designed with fire protection measures to mitigate the effects of fire. This may include using intumescent coatings on steel to delay temperature rise and the application of high thermal resistance concrete. Additionally, analysis and design consider the combined behaviour of materials under fire conditions, ensuring an integrated and efficient response.

Continuous research and development in composite structures exposed to fire aim to enhance design techniques, material selection, and fire protection strategies, aiming to increase the safety and resilience of these structures in emergencies. The objective is to ensure that composite structures can withstand extreme thermal demands during a fire, maintaining structural integrity and the safety of occupants.

The finite element method (FEM) is a powerful and widely used tool in structural analysis, including the assessment of the thermal behaviour of structures, such as composite slabs during a fire. The FEM is a numerical technique that divides a complex structure into discrete elements, allowing for detailed modelling and analysis of thermal and mechanical conditions.

In order to determine the temperature of a composite slab during a fire, the FEM is employed to simulate the thermal behaviour of the structure over time. Thermostructural modelling involves considering the variation of thermal properties of

materials with temperature, as well as the nonlinear effects that arise with the boundary conditions.

In this context, this dissertation investigates the impact of temperature on the flexural moment of composite slabs, utilising a new proposal grounded in the finite element method. The numerical validation of the developed model for the thermal analysis of composite slabs exposed to fire is performed using the ANSYS software.

1.1. Objectives

This study aims to investigate the impact of temperature on the sagging moment of a composite slab with steel deck, seeking to understand how thermal variations influence the bending resistance of the structure. A thorough analysis will be conducted to examine the specific thermal effects that affect the behaviour of the composite slab, particularly concerning the sagging moment.

As a significant part of this work, the intention is to propose a new formula for calculating the temperature in each relevant component. This innovative formula will be developed to provide a more precise and comprehensive approximation of the thermal effects on the individual components that make up the composite slab. The emphasis will be on the meticulous consideration of how temperature interacts with each element of the structure, thus influencing its ability to withstand load.

By proposing an enhanced formula, the goal is not only to advance the understanding of the thermal behaviour of the composite slab but also to provide more effective tools for calculating and predicting the effects of temperature on flexural resistance. This contribution may have significant implications in the field of structural design, offering engineers and designers a more solid foundation for addressing the specific challenges associated with thermal variations in composite slab structures

1.2. Thesis Description

This study is divided into a number of stages, the first being the development of a computational model, using the finite element method through ANSYS software, incorporating a non-linear thermal analysis, which can describe the behaviour of the COFRADAL 200 slab when subjected to fire during 120 minutes. The second stage consists of validating this computational model by comparing the computational results with the experimental results presented in the CSTB reports (Duponchel, 2006, 2011).

After validating this model, the investigation moves on to a parametric analysis involving various slab geometries, employing different thicknesses of rock wool as insulation material, a flat steel deck with steel ribs varying in strength, different reinforcement diameters, while also examining various concrete thicknesses. The methodology for the solution requires characterising the materials at elevated temperatures and incorporating an additional interface model. This model introduces thermal resistance between the steel deck and the covering material (rock wool), commonly referred to as the air gap effect, a phenomenon frequently observed during experimental tests. At the conclusion of the parametric analysis, this study proposes a novel approach to estimating the average temperature values of each component, based on the procedure outlined in Annex D (European Committee for Standardization, 2004).

2. LITERATURE REVIEW

Thermodynamics, which studies phenomena such as heat transfer and the conversion of energy into thermal energy, emerged during the Industrial Revolution to increase the efficiency of steam engines. This field has evolved to include four Fundamental Laws, which describe the characteristics of thermodynamic systems and the exchange of energy as heat or work (Atkins & de Paula, 2010). These principles are crucial in civil and materials engineering, where thermal conductivity is used for thermal analysis. Achieving thermal equilibrium requires the transfer of heat between bodies with different temperatures, according to the zero law of thermodynamics, and the second law is evident in the propagation of thermal energy from the hotter body to the colder one.

In construction, thermal analysis deals with gradual changes in ambient temperature and the effects of temperature gradients on the thermal expansion coefficients of materials, resulting in volumetric changes that can generate internal forces in hyperstatic structures. Thermal analysis is essential for ensuring structural fire safety, as heat flow and temperatures in structures evolve over time, altering the thermal and mechanical characteristics of materials until the elements reach a critical temperature.

In 1961, the International Organization for Standardization (ISO) established a committee to create a set of specifications for conducting fire resistance tests, leading to the initial design of the standard temperature-time curve . This design aimed to achieve consistency between the American ASTM E119 (American Society for Testing and Materials, 1918) and the British BS 476 (British Standards Institution, 1932) curves. The first version of this standard curve emerged as a result of this collaboration. In 1975, the ISO 834 standard titled *Fire-Resistance Tests - Elements of Building Construction* introduced a standardized fire curve with global applicability . This effort also influenced the development of nationally standardized fire curves in various countries, exemplified by Australia's AS 1530 (Standards Australia, 1994).

Later, in 1999, the ISO 834 standard underwent a revision that redefined certain test requirements and specifications for measuring instruments and instrumentation. This revision led to the introduction of ISO 834-1. Nevertheless, the tests recommended by ISO-834 proved to be expensive and time-consuming. Consequently, there arose a need to formulate calculations for determining the fire resistance of steel and concrete.

The initial technical standard proposing calculations for the fire resistance of composite steel/concrete slabs emerged in Europe in 1983, as introduced by ECCS 1984. This standard aimed to provide a method for assessing structural safety without the necessity of conducting experimental tests, aligning with the fire resistance classes outlined by ISO 834-1.

The commercialisation of composite steel/concrete deck slabs gained momentum in the United Kingdom in 1980. Despite having been employed in North America for two decades, concerns arose among the United Kingdom and European regulatory agencies. The reason for this unease was the perceived inadequacy of the data available up to that point to fulfil the fire safety criteria outlined in European standards. Consequently, Cooke et al. (1988) demonstrated that composite slabs could withstand fire for as long as 90 minutes by employing only a concrete reinforcement mesh. Prior to this, meeting such resistance criteria typically necessitated the use of reinforcing bars. These studies were grounded in experimental tests conducted between 1983 and 1985 by the British Steel Corporation (BSC) and from 1984 to 1986 by the Construction Industry Research & Information Association (CIRIA). The research findings indicated that slabs with a reentrant shape exhibit superior thermal shielding and insulation capabilities compared to trapezoidal ones.

Ralph Hamerlinck observed that the structural analysis recommended by ISO 834 was both expensive and time-consuming. Additionally, he noted that the calculation model proposed by ECCS 1984 was exceedingly conservative regarding structural safety. He anticipated the development of a mathematical model that could facilitate the calculation of the fire resistance of composite concrete/steel slabs with steel decks. Hamerlinck, therefore, put forth a numerical calculation model comprising three distinct numerical models in the paper titled "A numerical model for fire-exposed composite steel/concrete slabs", published in 1990. The design encompasses a structural analysis model for composite slabs, along with thermal and mechanical models for the analysis of the cross-section. Experiments conducted by the Institute for Building Materials and Structures (TNO) validated the model. Subsequently, in 1991, Hamerlinck published the book "The behavior of fire-exposed composite steel/concrete slabs", wherein he comprehensively outlined all the techniques utilised in constructing his calculation model.

In 1997, Kees Both developed a finite element model utilising the DIANA software to investigate the thermal and mechanical behaviour of Slim Flor systems

under fire exposure. The Slim Flor system, characterised by a steel deck and a concrete slab, exhibits a noteworthy phenomenon identified by Both when subjected to fire conditions with temperatures surpassing 100ºC. At this point, the concrete undergoes moisture evaporation. Alongside the finite element model crafted by Kees Both, a more in-depth exploration of the thermal characteristics of the Slim Flor system involved the incorporation of heat transfer mechanisms, including radiation and convection, within the void layer situated between the steel deck and concrete. These mechanisms play a pivotal role in the heat transfer during a fire event. Experimental tests conducted on Slim Flor systems served as a means to validate the numerical model. The comparison between the obtained experimental results and the predictions from the finite element model allowed Both and his team to ascertain the accuracy and reliability of the numerical simulations. Following the validation phase, a comprehensive parametric study was undertaken with the validated model. This study meticulously explored various parameters, encompassing material properties, dimensions, and fire scenarios, to scrutinise their effects on the thermal behaviour of Slim Flor systems. The outcomes of this thorough examination empowered Both to articulate succinct calculation rules and guidelines for the analysis of Slim Flor systems under fire conditions. With the establishment of these calculation rules, the thermal analysis of Slim Flor systems underwent a notable improvement in both speed and efficiency. This not only led to a reduction in costs associated with the construction system but also provided contractors and engineers with a practical tool. They could now rely on these simplified rules to assess the thermal response of Slim Flor systems to fire without engaging in expensive and time-consuming numerical simulations for each project.

Wald et al. (2006) reported several findings from a research project in their paper. The focus of this project was an experimental program designed to scrutinise the structural behaviour of an eight-floor steel/concrete composite frame building. The project encompassed seven large-scale fire tests conducted at different locations within the experimental building. Most of these tests involved a natural fire test analysis to explore the temperature evolution within various structural elements. A comprehensive description of each test is provided in "The Behaviour of Multi-Storey Steel Frame Buildings in Fire" (1999). These experiments were carried out by the Building Research Establishment (BRE) at the Cardington Laboratories steel test structure, constructed in 1993. The building had a plan dimension of 21 x 45m and a

height of 33m. To simulate the mechanical load, sandbags were added in addition to the structure's self-weight. As the structure did not collapse during the tests, it affirmed the conservative nature of the Eurocode fire design (2005). The conclusion drawn was that the configuration demonstrated satisfactory fire safety conditions. Essentially, a standard office building model, for which the load distribution arrangement was designed, exhibited similar resistance characteristics under fire conditions. In addition to these assessments, the results from the experimental tests were leveraged to conduct a detailed study of the connections between slabs, beams, and columns. This, in turn, contributed to refining analytical and numerical calculation models. During tests 1-3 of the experimental fire tests conducted at the Cardington Laboratories, only a limited number of temperature measurement points were recorded across the depth of the slab. In essence, there is a limited understanding of the temperatures reached within the slab during these specific tests. In addition to the aforementioned information, it's worth noting that in test 4, no temperature data was recorded within the slab. Recognising these limitations, Lamont S. et al. (2001) addressed this gap by utilising the finite element program HADAPT in 2001 to conduct a numerical heat transfer simulation. This simulation served to complement the experimental data by providing a comprehensive 2D nonlinear transient thermal study. The calibration of this model was conducted using the data from Tests 1-3, and its application to Test 4 allowed for the prediction of slab temperatures. While the model exhibited commendable performance, accurately simulating the results of Tests 1-3 and providing an accurate forecast for Test 4, it's noteworthy that the model tends to overestimate steel temperatures. On the other hand, its predictions for concrete temperatures are notably accurate.

In 2001, Gillie et al. (2011) developed a methodology for modelling composite floor slabs under fire conditions using a stress-resultant approach. The research aimed to analyse and predict the behaviour of concrete slabs at high temperatures, with a specific focus on the floor slab from the Cardington fire tests. Two software programs were employed to achieve this. The first software, known as SRAS (Stress Resultant Analysis of Structures), facilitates the analysis of the slab's stress and strain responses under various loading conditions. The second software, FEAI (Fire Engineering Analysis Interface), was instrumental in constructing realistic structural models and facilitating their analysis under fire conditions. This program enabled the researchers to explore the structural response of the models when subjected to fire scenarios. The

primary focus of the study was on utilising SRAS to analyse the behaviour of the floor slab based on the Cardington fire tests. The researchers aimed to assess the performance of the slab under different load conditions. The stress-resultant approach provided a suitable methodology for evaluating and modelling the behaviour of concrete slabs at elevated temperatures.

In 2002, Gillie M. et al. conducted a structural analysis of the third Cardington test employing the results obtained from the FEAST program. This program incorporates a user-defined subroutine compatible with ABAQUS finite element software, allowing the specification of the behaviour of shell elements through a stress-resistance approach. The analysis of the model revealed that in a fire scenario, the structural response is primarily influenced by thermal expansion effects. On the other hand, the impacts of cracking and gravity loading require time to begin affecting the structural behaviour. Nevertheless, at extremely high temperatures, a notable effect in composite slabs is the tensile action on the reinforcement mesh. During this phase, gravity loads directly influence the magnitude of the tensile forces in these elements. Examining the thermal gradients throughout the depth of the slab uncovered substantial interference at heightened temperatures, particularly after the steel deck had significantly diminished in resistance. These thermal gradients generated hogging moments, contributing to an escalation in deflections within the slab. Moreover, these thermally induced hogging moments might manifest in geometrically sagging regions. Consequently, the authors assert that to enhance the performance of composite structures and preserve structural integrity during fires, it is imperative to ensure adequate ductile reinforcement in concrete slabs.

L. Lim et al. (2004) developed a numerical model using the nonlinear finite element SAFIR program. Their study focused on assessing the fire behaviour of two-way reinforced concrete slabs following exposure to the ISO-834 standard test fire. The authors utilised a comparison with experimental testing of two-way reinforced concrete slabs exposed to fire, which they had previously conducted, to validate the model from 1992. Overall, a convergence was observed between the experimental testing and the 3D assessments of two-way reinforced concrete slabs modelled with SAFIR quadrilateral elements. The two-way slabs with simple supports demonstrate robust fire resistance in both scenarios, owing to their double curvature deformation and uniform support on all four sides. Additionally, the early development of tensile membrane action contributes to the remarkable performance of these slabs in fire

conditions. However, predicting the behaviour of the composite slab with the steel deck posed challenges.

Accurate modelling of the debonding effect and meticulous attention to detail are imperative for reasonably accurate results. This type of construction is considered one of the most promising cases for exploring the inherent fire resistance of composite structures through analytical design. Composite slabs exhibit compliance with rigorous regulations and fire resistance requirements, making them an advantageous subject for investigation. Researchers often employ experiments and validation model development using composite steel-concrete slabs to ascertain structural integrity during fire conditions.

In 2006, Wang A. J. and Chung K. F. conducted three standard ISO-834 fire tests named CS1, CS2, and CS3. These tests evaluated the structural performance of simply supported composite slabs under fire conditions, utilising reentrant profiled steel decking. The composite slabs used in the testing were fabricated with varying concrete thicknesses and quantities of bottom rib steel reinforcement to achieve fire resistance periods of 1, 2, and 3 hours. Through testing, the researchers evaluated the fire resistance of the slabs based on the load-bearing (R) criterion. Additionally, they determined the maximum displacements and maximum displacement rates of the slabs.

Until recently, both theoretical and experimental research examining the impact of fire on structures focused on evaluating structural behaviour during the heating phase of fires. Traditionally, theoretical and experimental research addressing the impact of fire on structures has primarily concentrated on assessing structural behaviour during the heating phase, as reflected in internationally accepted standard fire tests. However, it's imperative to acknowledge the equal significance of the cooling phase in ensuring structural safety under fire conditions. Fire tests conducted in real buildings have demonstrated that structures can withstand the heating phase but may fail during the cooling phase. Consequently, Bailey C. G. and Guo S. (2011) investigated the behaviour of composite slabs during both the heating and cooling phases, comprehensively covering all phases of a fire. During the experiments, nine identical composite steel-concrete slabs, consisting of steel mesh, normal-weight concrete, and trapezoidal metal decking, were tested. The remaining two slabs underwent examination at ambient temperature. Among these, seven slabs were assessed under diverse fire conditions, encompassing both the heating and cooling

stages. The structural behaviour was analysed using three distinct fire scenarios, each representing various heating regimes. In the initial scenario, the furnace underwent a 40-minute heating phase, reaching a temperature of 950 °C, followed by a cooling stage. The second scenario entailed a 90-minute heating process to achieve 800 °C, followed by cooling. The third scenario involved a gradual cooling process, similar to the first scenario's heating, but with the cooling fans turned off, resulting in slight variations. For fire scenarios 1 and 2, the slabs underwent testing with applied static loads of 72, 44, and 12 kN. These loads were representative of typical real-load scenarios, providing insight into various structural reactions. In the case of fire scenario 3, only one test was conducted with a 44 kN applied load. The results from the study indicated that fire scenario 1 exhibited the most significant vertical displacement during heating. This displacement was influenced by the thermal curvature and the temperature of the steel deck. In contrast, for fire scenario 2, the cooling phase occurred when the slab's top surface had reached its maximum temperature. The longer duration of the heating phase allowed the slab more time to conduct heat. Notably, among all the experiments, the mesh reinforcement in fire scenario 2 experienced the highest temperatures. The scientists found that both the applied stress and the temperature to which the slabs are subjected influence the vertical displacement of the slab. Regarding residual displacement, it was observed that the cooling time directly affects the extent of residual displacement.

Continuing the research efforts to encompass both the heating and cooling phases of composite slabs under fire situations, Guo S. (2012) presented a study to validate the numerical models developed in this paper, the author conducted experimental fire tests on seven trapezoidal steel decking composite slabs under various fire exposure conditions. These tests were previously detailed and conducted by Guo S. and Bailey C. G. at the University of Manchester in 2011. Subsequently, two nonlinear finite element models were developed using ABAQUS software, to simulate the thermal and mechanical behaviour of composite steel and concrete slabs during both the heating and cooling phases. A constant longitudinal temperature distribution was assumed to streamline the thermal model. This simplification enabled the creation of a plane model, reducing the interaction between steel and concrete to a thin layer. As part of the model simplifications for simulating the slab in structural analysis, a narrow strip with a width of 180 mm was incorporated. Nonlinear spring elements were employed to simulate the interaction between the steel deck and concrete, while solid

elements (C3D8), shell elements (S4R), and truss elements (T3D2) were used for modelling the concrete, steel sheeting, and mesh, respectively. The results indicated that the reaction force of composite slabs exhibits significant amplitude fluctuations during both heating and cooling phases, influencing the distribution of structural loads. The structural analysis revealed that the steel deck yielding and concrete fracture may reduce the internal stress induced by thermal expansion. This suggests that constrained constructions at high temperatures may benefit from the weakening of composite slabs. Additionally, a parametric analysis was conducted to examine how the thickness of the steel deck, the size of the reinforcement mesh, and the strength of the concrete would impact the behaviour of composite slabs in a fire. This investigation demonstrated that the thickness of the steel deck significantly influences the behaviour of the composite slab, while the mesh size and concrete strength have only a minimal impact.

Piloto P. et al. conducted a study in 2018 analysing the fire resistance of composite concrete slabs with a profiled steel deck, typically reinforced by a steel mesh at the topside, including reinforcing bars between its ribs. This structural solution is commonly employed in various types of buildings. However, it was essential to verify its safety under fire situations. The design validation is usually carried out using the ISO-834 standard fire curve, considering criteria for stability (R), insulation (I), and integrity (E). Due to the high cost and time-consuming nature of experimental testing, fire resistance can also be assessed using numerical simulation or straightforward mathematical procedures. The insulation fire resistance (I) has been determined by computational models and simplified calculation methods. Alternative trapezoidal geometry combinations were tested to assess the impact of the thickness of the concrete and steel deck. Based on their findings, the authors demonstrated that both calculation methods led to an increase in fire resistance (I) as concrete thickness increased. However, the numerical method predicted a lower fire resistance (I) than simple calculation methods, thereby enhancing structural safety. The fire resistance was consequently defined using a new, safer design formula.

In 2019, Piloto P. et al. investigated the thermal behaviour of composite steel concrete slabs under standard fire test conditions. The slab's structure comprises a steel deck covered by a concrete layer and a top mesh. To resist positive bending, individual rebars were placed between the ribs. Numerical analyses were conducted using computer models developed in ANSYS and MATLAB. The 3D models were

studied through nonlinear thermal and structural analysis using finite elements. Consequently, the numerical validation for the load support (R) and insulation (I) criteria was established. The thermal model incorporated an air gap between the steel deck and concrete to simulate the debonding effect. Initially, the thermal and mechanical 3D models were validated against experimental data, regarding the insulation (I) and load-bearing (R) models. These results were also compared to the simplified calculation model of Eurocode 1994-1.2. This analysis revealed that Eurocode 1994-1.2 overestimated the fire resistance, yielding potentially unsafe results. These authors also notice that when using perfect contact between the steel deck and the concrete, the numerical results underestimate the fire resistance, demonstrating that models accounting for the debonding effect are more accurate. A new calculation formula was developed to determine the insulation fire resistance, enhancing the current calculation techniques.

Juan Coz-Díaz and Juan Martínez-Martínez (2020) conducted an investigation involving the experimental study of lightweight concrete (LWC) and normal weight concrete (NWC) composite slabs with steel decking profiles exposed to a standard ISO834 fire. This study compares the fire behaviour of NWC with LWC composite slabs. The dimensions of the slab were 160 mm thick, 1120 mm wide, and 2030 mm long. To conduct fire tests on intermediate-scale samples, a non-standard furnace was designed and assembled. The furnace consists of a heating chamber, an exhausting system, and a portal frame. The heating chamber is constructed with a steel framework and refractory layers. The exhausting system was responsible for extracting hot gases. The portal frame is made up of steel profiles with a rotating beam equipped with a linear actuator to apply the load on the samples. This beam can be opened to facilitate the placement of the slabs and closed during the test.

Paulo Piloto and Carlos Balsa (2020) used ANSYS to conduct a simulation and present a new sophisticated computational approach. Following the validation of the numerical model using experimental data from the literature, a parametric analysis was performed to understand better the impact of the load level on the composite structure under fire. To validate the simulations, three different models were employed: the first model assumes perfect contact between the steel deck and concrete topping, while the two succeeding models assume the presence of an air gap between these materials, acting as a thermal resistance on the temperature field throughout the thickness of the slab. The numerical results exhibit good agreement with the

experimental results, particularly when utilising the non-perfect contact model, with differences of 3.88% and 16.91% concerning the insulation and load-bearing criteria, respectively. These authors also developed a parametric study, changing the load level from 10% up to 75%. New simple calculation models were also introduced to determine the fire resistance of composite slabs, taking into account the load level and the debonding effect between the concrete and the steel deck.

In 2021, Bolina et al. investigated the temperature distribution in the cross-section of steel decking concrete slabs subjected to fire using three different procedures: experimental, numerical, and analytical methods. The authors conducted experimental tests corresponding to eight real-scale fire tests on slabs. These tests were utilised to calibrate numerical models using Abaqus. The analytical methods employed were those proposed in Annex D of EN 1994-1-2. The analytical temperatures of the steel decking exhibited convergence with the experimental and numerical results. However, the same was not observed for the concrete, positive and negative rebar, and thermal insulation temperatures.

In 2006, the company Arcelor Mittal requested CSTB, represented by Xavier Duponchel, to carry out a study. The aim was to estimate the duration of fire resistance of the COFRADAL 200 floor in six different configurations in terms of reinforcing steel section, loading and span. The approach taken to carry out the study followed 3 steps: the first was to model the thermo-mechanical behaviour of the COFRADAL 200 sidewalk tested under fire conditions, the second was to compare the results of the calculations and the measurements made during the test (temperatures and deformations) to validate the calculations made with SAFIR and finally to model and estimate the duration of the slabs fire resistance in each of these configurations. The floor configurations studied have a fire stability of 60 or 120 minutes. Furthermore, during the fire resistance test, this floor maintained its thermal insulation for the entire duration of the test (120 minutes). Consequently, the floor configurations studied can be classified as REI60 or REI120 depending on the case.

In 2011, in order to continue the work developed in 2006, Arcelor Mittal request a new study, again led by Xavier Duponchel. As part of the request to renew the technical opinion on the COFRADAL integrated insulating floor process, Arcelor Mittal wanted to extend the range of floors with different thicknesses and a “reinforced” range with higher concrete ribs. Arcelor Mittal then requested CSTB to study 4 configurations of its ranges: The 200, 230 and 260 versions of the “Standard” range (STD) and The

230 version of the “reinforced” range (R230). The study also included the thermal analysis, enabling the calculation of the temperature inside the sections and then calculate their duration of fire stability.

These last two studies served as the basis for this dissertation. The results of the experimental tests carried out in 2001 and 2003, set out in test reports RS01-156 and RS02-092, were used to validate the new computer model proposed in this research, which considers the occurrence of a detachment between the steel deck and the rockwool, creating the air gap effect.

3. COMPOSITE SLABS UNDER FIRE

When investigating composite slabs under fire, it is essential to understand the variables that influence the most these structural elements and may result in reductions in strength and stiffness (Buchanan, 2001). The proper assessment of structural resistance under fire, whether analytically, numerically, or experimentally, depends on the evolution of temperature over time, with significant variations for various fire scenarios.

The effects of temperature increase on a structural element, especially steel and concrete, are much more complex than at ambient temperature. This chapter will present some of the variables used in formulating the mathematical model of physical phenomena that prescriptive codes employ to design a structural element in a fire situation.

3.1. Geometries

Experimental fire testing is typically expensive and time-consuming. However, numerical modelling and simple mathematical methods can be used to assess the fire resistance of composite panels. When exposed to fire, the presence of ribs complicates the evaluation of the cross-sectional temperature field in composite slabs. Calculating the unexposed surface temperature and predicting the fire resistance of composite slabs are challenging aspects in fire protection design.

The Figure 1 presents the initial geometry of the studied composite slab under analysis. This composite slab is made by special steel deck, rockwool, concrete and rebars. Each steel deck has a width of 600 [mm], and the left edge connects to the right edge of the second steel deck. This figure also includes an approximate geometry, used to develop the finite element model.

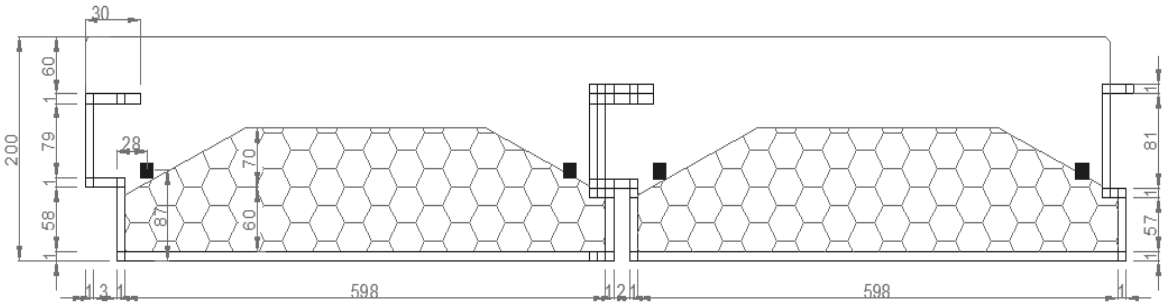

Figure 1- Studied geometry, COFRADAL 200 composite slab.

The slabs is made of a 1 mm thick steel deck, with 600 [mm] of width and a height of 140 [mm]. Additionally, the slabs include 130 [mm] of rockwool thermal insulation, 16 [mm] reinforcement bars, and 60-70 [mm] of concrete. In Chapter 5, the modifications made to the original geometry, which led to the parametric analysis, will be presented.

The Figure 2 provides a detailed representation of the terminology adopted for the main components of the composite slab geometry. In this cross-sectional view, the structural elements that make up the system are highlighted, including the regions known as the *upper flange* and *lower flange*, which correspond to the upper and lower portions of the profiled steel section. These flanges play a fundamental role in flexural resistance and in the overall behaviour of the slab under thermal and mechanical loads.

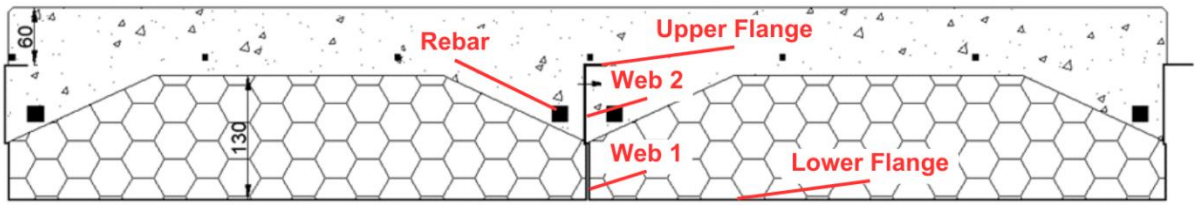

Figure 2 - Identification of the main structural components of the composite slab cross-section.

The internal parts of the section, designated as web 1 and web 2, act as vertical webs connecting the flanges, significantly contributing to the bending stiffness and structural integrity of the assembly. They also define the space allocated for the rockwool thermal insulation. Additionally, the position of the steel reinforcement bars (rebar) embedded in the upper cast-in-place concrete layer is included, highlighting their primary function of resisting tensile stresses and enhancing the slab's performance under fire exposure and normal service conditions.

3.2. Fire

To determine the rise in temperature in a structural element, it is first necessary to establish the amount of heat reaching that element. R. Rigobello (2007) emphasises that correctly determining the thermal actions on structural elements requires understanding the mechanisms by which heat is generated and propagated within an environment. In this regard, Twilt et al. (1994) argue that the time a structural element can withstand depends directly on the temperature rise itself. The temperature evolution depends on various factors, such as the amount of combustible material present and the ventilation conditions of the environment.

For this reason, considerable efforts have been made to formulate mathematical models that describe the evolution of fire temperature over time. According to Costa e Silva (2006), this relationship between temperature and time is represented by fire curves. When standardised, these curves are called "standard curves"; when parameterised according to the characteristics of the fire scenario, they are called "natural curves".

3.2.1. Natural Fire Curve

The natural fire, as noted by R. Rigobello (2007), is the fire model where the gas temperature follows temperature-time curves constructed from fire tests that simulate the real situation of a compartment engulfed in flames. The results of these tests depend on parameters such as fire load, degree of ventilation, and thermal characteristics of the sealing material.

Fire characterisation depends simultaneously on three factors: a heat source, the fuel, and the oxidiser, which is typically oxygen. Figure 3 represents the temperature rise curve over time for a real fire.

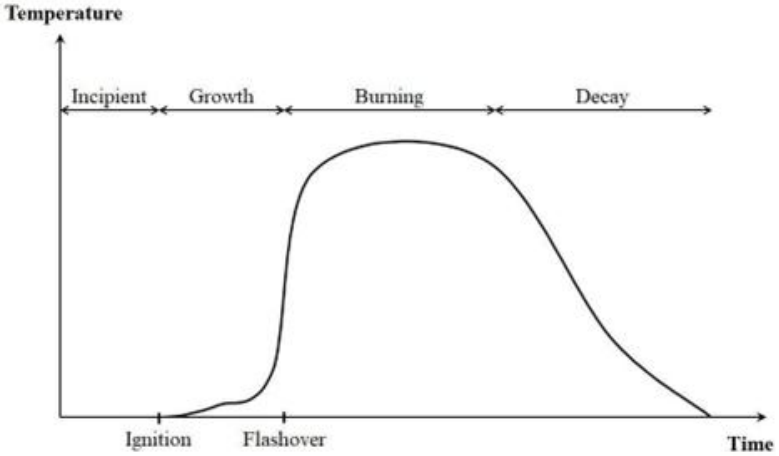

Figure 3 – Curve of a real fire Rigobello, 2007.

In a fire, four distinct phases are usually identified and distributed across the regimes of ignition, propagation, and extinction. The initial phase, or ignition, is characterised by low temperatures and the production of toxic gases. During this phase, the rise in temperature does not affect the structural behaviour of the building. In the second phase, known as propagation, the temperature is rising. During this phase, there is a sudden ignition of gases, and heat transfer occurs predominantly through radiation and convection. Temperatures in the hottest zone of the fire compartment range between 450 [ºC] and 600 [ºC], or there is a heat flux of 20 [kW/m²] at ground level. At this moment, the phenomenon known as "Flashover" or generalised fire occurs. The third phase is the full development of the fire, where temperatures can further increase, and the material is in complete combustion. The fourth phase is the cooling and extinction of the fire, due to the progressive decrease in the temperature of the gases, either because of a lack of fuel load, oxidiser, or due to external intervention.

3.2.2. Nominal Fire Curves

The EN 1991-1-2, published by CEN (2002), proposes three nominal fire curves: the ISO 834 standard fire curve, the hydrocarbon curve, and the external elements fire curve. For the sake of objectivity, the standard ISO834 fire model, which is the focus of this study, will be detailed. Figure 4 illustrates the three nominal fire curves superposed.

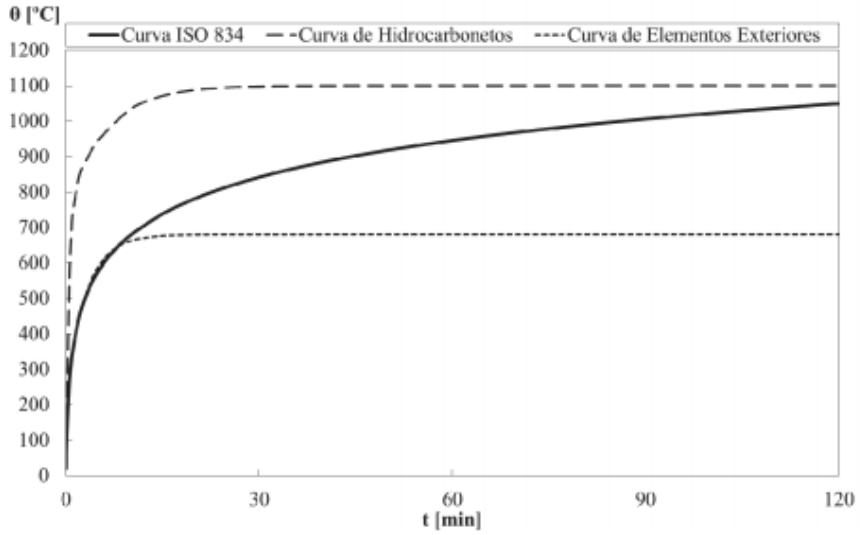

Figure 4 - Nominal fire curves by EN1991-1-2.

According to Franssen and Vila Real (2010), the temperature curve as a function of nominal time is an analytical mathematical representation of a continuous function. This curve is considered an arbitrary convention of temperatures present in a real fire, regardless of the type or dimensions of the building. The standard fire is an idealised model of temperature rise as a function of time, used for experimental analysis purposes. It ensures that the collapse of the element occurs at the maximum test temperature value. According to Wang, although the standard fire is a simplification of a real fire model, several studies on the behaviour of mixed steel and concrete elements at high temperatures have been conducted using this model. Therefore, it is widely used for structural research in fire situations.

3.2.3. ISO 834 Standard Fire Curve

In 1975, the International Organization for Standardization (ISO), the worldwide federation responsible for standardising national standards bodies, established the international standard governing the methodology for fire resistance testing.

Aligned with ISO 834, the EN1991-1-2 , published by CEN (2002), supplies the equation for temperature increase over time using cellulose-based fuel. This equation serves as a guideline for assessing the fire resistance of diverse building components when exposed to standard fire conditions.

$$\theta_g = 20 + 375\ log\ log\ (8t + 1) \qquad [°C] \tag{1}$$

Where θ_g is the gas temperature in the compartment in flames in [ºC], t is the time in [min]. Assuming a convective heat transfer coefficient of α = 25 [W/mºK]. The equation predicts temperatures reaching 745 [ºC] within the first fifteen minutes of the fire, and increases by about 100 [ºC] with each doubling of time. Figure 5 presents the curve standardised by ISO 834.

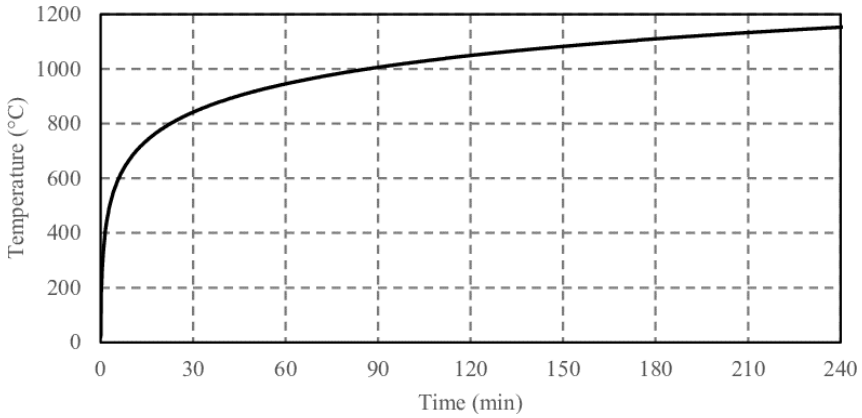

Figure 5 – Nominal time-temperature fire curves.

3.3. Heat Transfer

To better understand the mechanisms of heat transfer, it is essential to clarify some basic concepts. "Temperature" can be defined as the measure of the kinetic energy present in the molecules of a substance. In other words, it measures the coldness or warmth of a substance. Çengel and Ghajar (2006) define "heat" as the form of energy that can be transferred from one system to another due to a temperature difference.

In this context, Vila Real (2003) defines the process of heat transfer as the propagation of energy from one area to another through a solid, liquid, or gaseous medium, resulting from the temperature difference between them. This process occurs via conduction, convection, or radiation. The heat flow by radiation does not require any material support and heat transfer occurs by electromagnetic radiation.

As emphasised by R. Rigobello (2011), the temperature distribution in a medium is controlled by the combined effect of these three modes of heat transfer. The choice of the mode of heat transfer or their combination is, therefore, mandatory.

Thermal actions, as regulatory provisions, are defined EN1991-1-2 in terms of a heat flux density incident on the surface of the element. This is the sum of two components: convection and radiation, as shown in Equation 2.

$$\dot{h}_{net} = \dot{h}_{net,c} + \dot{h}_{net,r} \qquad [W/m^2] \qquad (2)$$

The following subsections present the formulation used to determine each component of the above equation and provide a brief description of the three modes of heat transfer.

3.3.1. Conduction

Conduction can be defined as the exchange of energy in the body from particles with higher energy levels (higher temperatures) to particles with lower energy levels (lower temperatures) due to cooperation between the particles. Thermal conduction movement can occur in solids, gases or liquids. This property is represented by Fourier's law of heat conduction, proposed in 1822. As this law shows, the conductive heat movement h (W/m²) is directly related to the temperature gradient $\frac{dT}{dx}$ (K/m), as expressed in the following:

$$\dot{h} = -\lambda \frac{dT}{dx} \qquad [W/m^2] \qquad (3)$$

In Equation 3, $\frac{dT}{dx}$ represents the temperature gradient in the direction of the heat flow [K/m] and λ is the thermal conductivity of the material [W/m.K], where:

$$-\frac{dT}{dx} = \frac{\dot{h}}{\lambda} \propto \frac{1}{\lambda} \qquad (4)$$

Equation 4 helps us understand that the thermal conductivity property that appears in the Fourier equation. It is a property of each material and represents how easily it conducts heat. The values can vary widely depending on the chemical composition, physical state and temperature of the material.

The negative sign in the formula is due to the fact that the temperature increases in one direction, while the heat flow occurs in the opposite direction, from higher to lower temperature, thus ensuring a positive heat flow.

Heat flow is a quantitative vector and therefore, acts in a three-dimensional field. Heat conduction is now represented by the following equation:

$$\vec{h} = -\lambda \cdot \nabla T \qquad [W/m^2] \tag{5}$$

In Equation 5, as clearly explained by R. Rigobello (2011), ∇T represents the gradient operator. According to Lienhard IV and Lienhard V (2017), the thermal conductivity is more complex and is rarely considered a constant because it also depends on position and temperature, even in homogeneous materials.

3.3.2. Convection

According to R. Rigobello (2011) convection is the mechanism of heat transfer between a solid and a fluid moving in the vicinity of that solid, once there is a temperature difference between them, in another words, heat transfer by convection occurs when energy is transferred between a solid and a moving fluid or gas, each at different temperatures. The rate of this energy exchange is described by Newton's law of cooling, as shown in equation 6:

$$h_{net,cv} = \propto_{cv} \cdot \left(\vartheta_g - \vartheta_m\right) \tag{6}$$

Where $\propto_{cv}$ is the coefficient of convective heat transfer (W/m²K), relevant for nominal temperature-time curves; ϑ_g denotes the gas temperature near the fire-exposed element (°C); and ϑ_m is the surface temperature of the element (°C). The value of the convection coefficient varies with the velocity of the fluid or gas and should

be taken as αcv = 9 (W/m²K) for non-exposed surfaces to simulate the radiation effect, αcv = 25 (W/m²K) for surfaces exposed to the ISO834 curve, and $\propto_{cv}$ = 50 (W/m²K) for surfaces exposed to hydrocarbons.

3.3.3. Radiation

Heat transfer by radiation is the only form that does not rely on a material medium to propagate and can heat even distant objects in an environment, including in a vacuum. Thermal radiation is heat transfer through electromagnetic waves, which propagate radially from the source at the speed of light.

According to Y. C. Wang (2002), radiation is the transformation of energy into electromagnetic waves, allowing a surface to absorb, transmit, or reflect the incident radiation. In this sense, the following equation represents heat transfer by radiation:

$$\omega + \Psi + \tau = 1 \tag{7}$$

In Equation 7, according to R. Rigobello (2011), the term ω represents the absorptance, Ψ the reflectance and τ the transmittance, which are functions of the temperature, wavelength and surface properties of the body.

The extreme case, where all thermal radiation is absorbed by the body, with $\omega = 1$, is considered an ideal body and is referred to as a black body. Black body radiation is fundamentally important to the study in question because it is a perfect emitter of radiation (Y. C. Wang). This means that no other body emits more thermal radiation per unit area than a black body at the same temperature. The total amount of radiation, E_b, emitted by the surface of a black body depends solely on its temperature and is given by the Stefan-Boltzmann law, as shown in the following equation:

$$E_b = \sigma \cdot T^4 \qquad [W/m^2] \tag{8}$$

In Equation 8, σ represents the Stefan-Boltzmann constant, whose assigned value is 5.67x10^{-8} [W/m²K], where T is the temperature on an absolute scale (in Kelvin).

It is evident that the idealized properties represented by the black body do not occur in reality, since no material emits and absorbs radiation perfectly. Generally, it is necessary to introduce an additional term to quantify the energy emitted by the surface of any body. This term is called emissivity, represented by the parameter ε. Emissivity is defined as the total energy rate emitted by a real surface divided by the rate emitted by a black body surface. Thus, emissivity can vary with values between 0 and 1. Therefore, the total radiant energy emitted by a real surface is given by the following equation:

$$E_b = \varepsilon\, \sigma \cdot T^4 \qquad [W/m^2] \tag{9}$$

Generally, the emissivity of a surface depends on the wavelength of the radiant energy, the temperature, and the angle of radiation. However, if the emissivity is assumed to be independent of these factors, the radiating surface is termed a gray body surface. Gray body radiation is widely used in fire safety engineering calculations.

The emissivity of steel and concrete materials is 0.7. The emissivity of fire (flames) is assumed to be 1.0. When not specified, the emissivity can be taken as 1.0.

Another relevant variable for calculating problems related to temperature rise is the view factor, which creates a shadow effect on the receiving surface. CEN - EN1993-1-2 and CEN - EN1994-1-2 recommend its application due to the obstruction of thermal radiation caused by the geometric shape of the steel profile.

For composite slabs with profiled trapezoidal or reentrant, the view factor relies upon the direction of surfaces and the distance between them. These view factors can be determined following the basic crossed-strings strategy, created by H. C. Hottel during the 1950s (2008). This approach is additionally embraced by the principles EN 1994-1-2.

The view factor of the lower flange of the composite slabs is given as Φlow = 1. It can be inferred from checking the opening of the coordinates caused by the ribs of the steel deck that the view factor of the core and upper flange is less than one due to the shading caused. However, in this study, the view factor for all regions was adopted as 1.0.

Considering all the variables that influence heat transfer, as defined in CEN - EN1991-1-2, the net heat flow affecting the surface of the element is shown by the following expanded equation:

$$h_{net} = \propto_{cv} \cdot \left(\vartheta_g - \vartheta_m\right) + \phi \cdot \varepsilon_m \cdot \varepsilon_f \cdot \sigma \left[\left(\vartheta_g + 273\right)^4 - \left(\vartheta_m + 273\right)^4\right] \quad (10)$$

Where ϑ_g, is the gas temperature of the compartment in [ºC] and ϑ_m, is the surface temperature of the element, also in [ºC].

3.4. Thermal Properties

3.4.1. Carbon Steel

The specific heat of steel is the amount of energy needed to raise the temperature of a unit mass of steel by 1 [°C], and it also indicates the material's capacity to absorb heat. According to Eurocode EN1993-1-2 (2005), the specific heat of steel, denoted as "Cp," is defined as shown in Figure 6.

Thermal conductivity is the coefficient that determines the rate at which heat reaching the surface of the steel is conducted through the material. According to Eurocode EN1993-1-2 (2005), the variation of thermal conductivity with temperature is shown in Figure 6, which also defines the density of steel as a constant equal to ρ = 7850 [kg/m³].

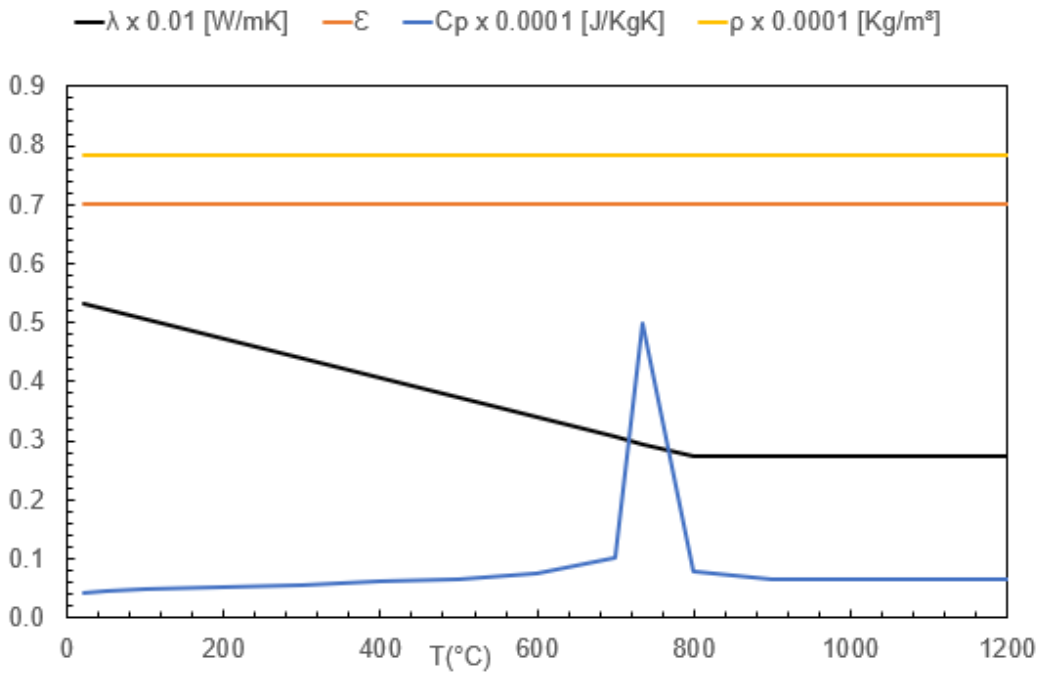

Figure 6 – Steel Thermal Properties.

The emissivity of steel, as previously mentioned, was adopted as 0.7. The graph in Figure 6 shows the thermal properties of steel that have been mentioned, namely specific heat, thermal conductivity, density and emissivity, all as a function of temperature variation.

3.4.2. Concrete

The specific heat of concrete (Cp) varies mainly with the moisture content. The moisture within the concrete causes a peak between 100 [ºC] and 200 [ºC] due to the water evaporation. Figure 6 depicts the variation of this property with temperature. The peak value depends on the amount of moisture, which was assumed to be 3%.

Thermal conductivity depends on the type of aggregate and the temperature of the concrete. The thermal conductivity “λc” of concrete can be determined between the lower and upper limit values. Figure 7 shows the variation of the upper limit of thermal conductivity with temperature according to Eurocode EN 1992-1-2. It is expected to have a different behaviour of this thermal property in the next generation of Eurocodes, which justifies the evolution of this property (CEN, 2021).

Density is a physical property of matter, qualitatively defined as the weight of objects with a specific volume, and is denoted by ρ. The common unit of density is

(kg/m^3). Figure 7 represents the variation of density with temperature according to the calculation suggested by Eurocode EN 1992-1-2 (CEN, 2004). The reference value for density at room temperature was taken to be ρ (20 ºC=2300 Kg/m^3).

The emissivity of concrete, as previously mentioned, was adopted as 0.7. The graph in Figure 7 shows the thermal properties of concrete that have been mentioned, namely specific heat, thermal conductivity, density and emissivity, all as a function of temperature variation.

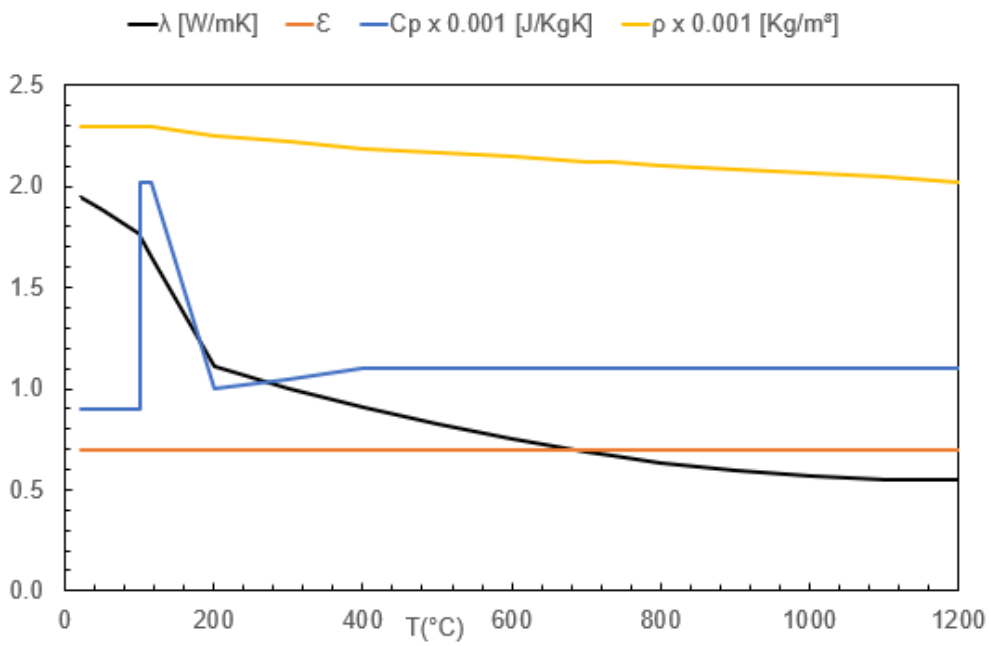

Figure 7 – Concrete Thermal Properties.

3.4.3. Rockwool

The emissivity of the rockwool, as mentioned previously, was adopted as 0.7. The graph in Figure 8 shows the thermal properties of stone wool, such as specific heat, thermal conductivity, density and emissivity of mineral wool, all as a function of temperature variation according to EN 1995-1-2 (2004).

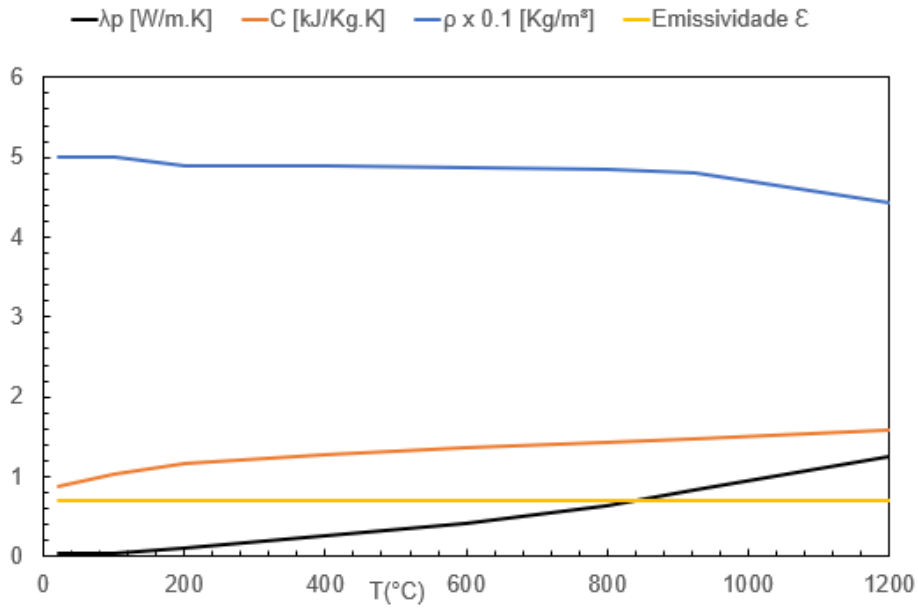

Figure 8 – Rockwool Thermal Properties.

3.4.4. Air

The thermal properties of the air depend on temperature and must be used to simulate the interface between the steel deck and the bottom surface of the rockwool. In addition, these thermal properties vary with air pressure. This work considers the thermal properties of air at 1 atm of pressure, and the data on the thermal properties of air are proposed by Cengel (2006) and are shown below in Figure 9.

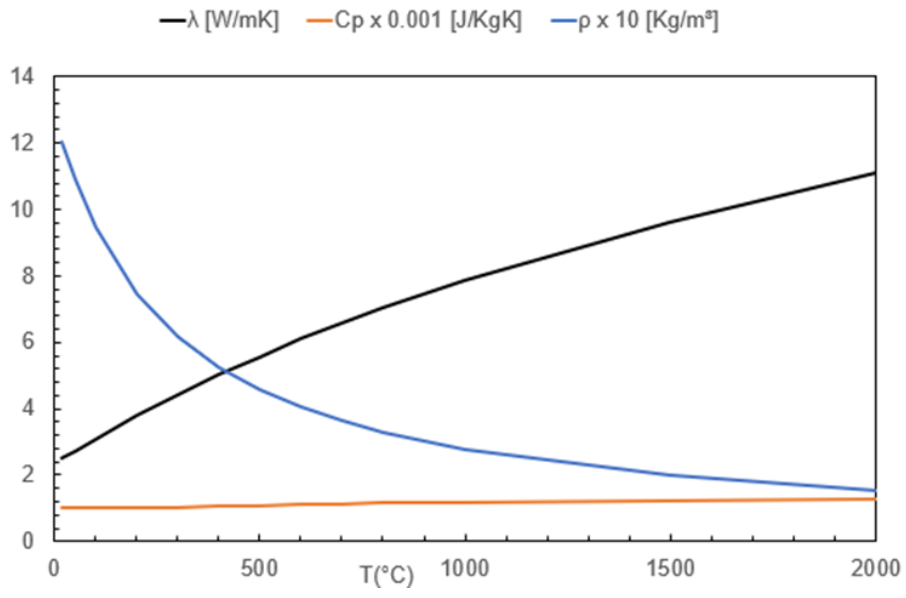

Figure 9 – Air Thermal Properties.

3.5. Mechanical Properties

3.5.1. Steel

Exposure of steel to high temperatures causes its physical and chemical characteristics to be modified, leading to a reduction in stiffness and strength (Martins, 2002). The equations 11 and 12 show how to calculate the reduction factors, in relation to the values at 20 [°C], for the yield strength and modulus of elasticity of structural steels at high temperatures, respectively, so that:

$$K_{y,\theta} = \frac{f_{y,\theta}}{f_y} \tag{11}$$

$$K_{E,\theta} = \frac{E_\theta}{E} \tag{12}$$

In these formulas, $f_{y,\theta}$ represents the yield strength of the steel at elevated temperature “θ”; f_y represents the yield strength of the steel at room temperature (20°C); E_θ is the modulus of elasticity of the steel at a temperature “θ” and finally, E is the modulus of elasticity of the steel at room temperature (20°C).

3.5.2. Concrete

At high temperatures, there is a significant reduction in the modulus of elasticity of concrete. This decrease can be explained by the rupture of the internal bonds between the cement matrix, where the Van der Walls forces between the layers of C-S-H (hydrated calcium silicate) are reduced (Kamal & Ghali, 2018). Schneider (1983) proposes a decrease in the modulus of elasticity as a function of temperature, according to the coefficients shown in Table 1.

Table 1 – Reduction coefficients of the modulus of elasticity of concrete as a function of temperature, Schneider, 1983.

TEMPERATURE (°C)	REDUCTION COEFFICIENT (K_E)
20	1
40	1
200	0,5
400	0,2
800	0,1
1200	0

The tensile strength of concrete is generally neglected at ambient and elevated temperatures. This is because concrete's main strength is in compression. In this case, increasing the temperature leads to a decrease in the compressive strength value (Kodur & Agarwal, 2014).

The compressive strength of concrete decreases with increasing temperature and can be obtained from the Equation 13.

$$f_{c,\theta} = k_{c,\theta} \cdot f_{ck} \tag{13}$$

Where, $f_{c,\theta}$ is the compressive strength of concrete subjected to temperature θ; f_{ck} is the characteristic compressive strength of concrete in the environment; $k_{c,\theta}$ is the concrete strength reduction factor at temperature θ.

4. THERMAL COMPUTACIONAL MODELLING

4.1. ANSYS

ANSYS is a general-purpose finite element software used to solve a variety of physical problems. These problems include static or dynamic structural analysis (linear and non-linear), heat and fluid transfer problems and acoustic and electromagnetic problems.

With ANSYS one can analyse models from the simplest to the most complex with extreme flexibility and the benefits of software already used by science and industry. The domain is subdivided into small discrete regions called finite elements (Figure 10). These elements are defined by geometric and mathematical entities, nodes. The method is based on interpolation functions and numerical integration methods (Coelho et. al 2014).

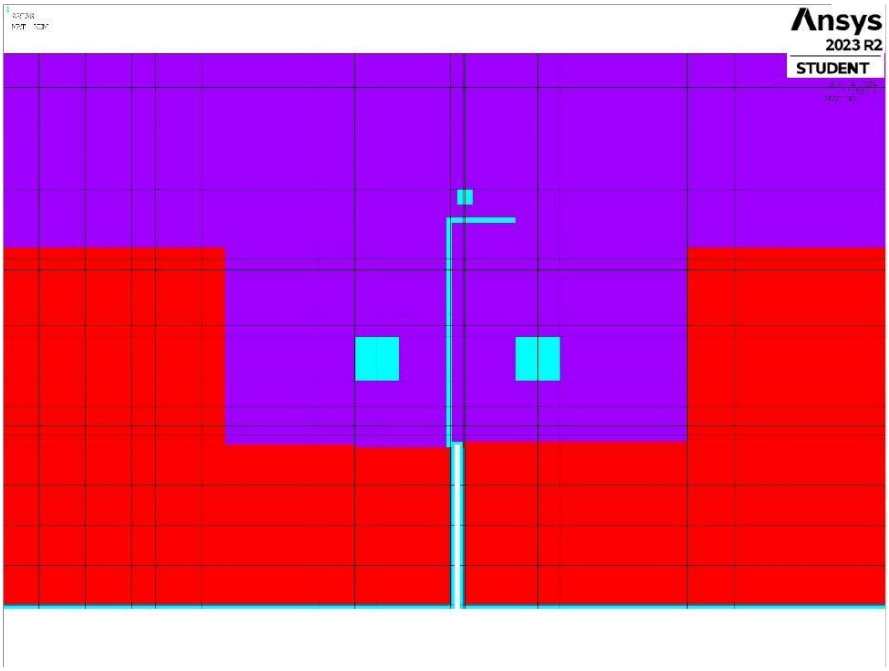

Figure 10 – Finite elements.

The PLANE 55 finite element, which has a two-dimensional (2D) thermal conductivity capacity, was used to analyse the thermal effects on the structure under analysis. The element has four nodes, each node has one degree of freedom,

temperature as it is shown in Figure 11. This element uses linear interpolating functions and full Gauss integration.

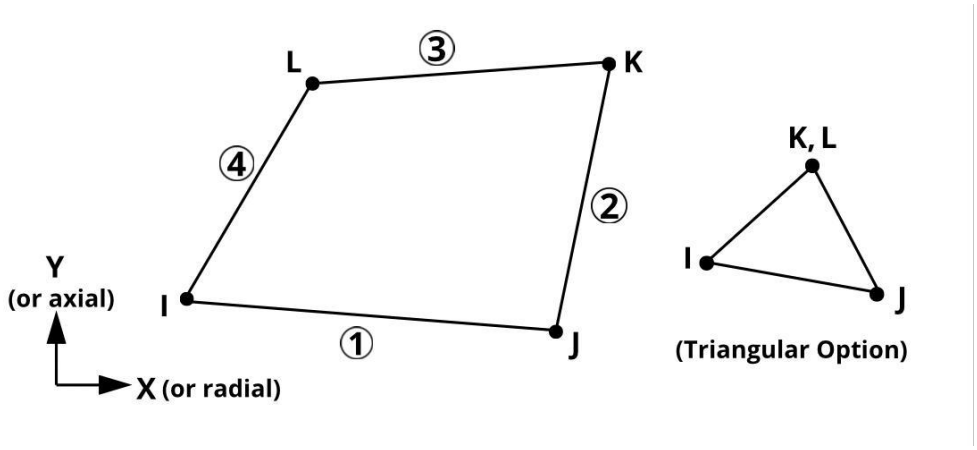

Figure 11 – Geometry of the PLANE 55 element (ANSYS library).

4.2. Boundary Conditions

A uniform initial temperature is applied to all mesh nodes (15ºC). The lower part of the slab is subjected to normal fire conditions, using a convection coefficient of 25 [W/m^{2}K] and a fire emissivity equal to 1. The upper part of the slab is subjected to a convection coefficient of 9 [W/m²K] to include the effect of radiation. These parameters are shown in Figure 12.

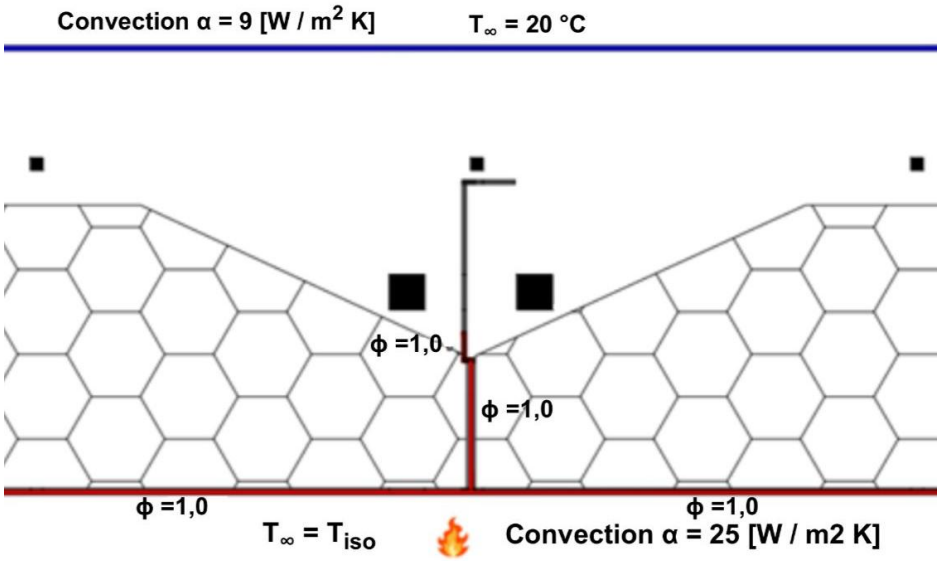

Figure 12 – Thermal boundary conditions.

4.3. Validation with Experimental Results

The main difference between the model proposed in this study and the model developed by X. Duponchel in 2006 and 2011 was the application of an air gap to simulate the detachment that occurred between the steel deck and the stone wool during the experimental tests. In addition, the SAFIR software was used in the above-mentioned study and ANSYS is the software chosen for this one. In the report developed by X. Duponchel, ten different temperature measurement points were selected throughout the 120-minute fire test. Figure 13 presents the parametric dimensions, while Figure 14 below shows these selected points, which were used to compare the results and subsequently validate the computer model developed. In section 4.4, comparative graphs will be presented between the results of the computational model proposed by X. Duponchel, the experimental results and also the results of the computational model proposed in this work using the ANSYS software. Finally, the root mean square error will be presented for each of the ten points, thus proving the validity of the model presented.

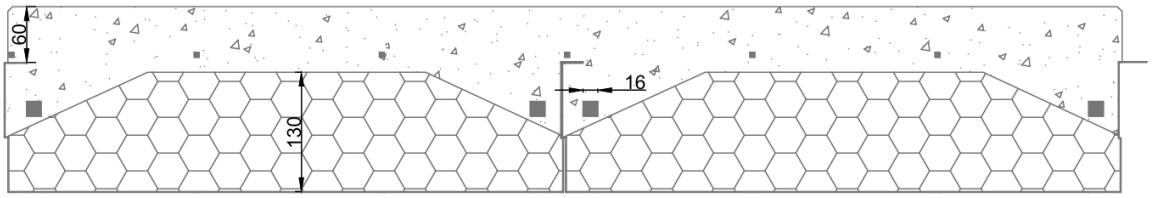

Figure 13 – Parametric Dimensions.

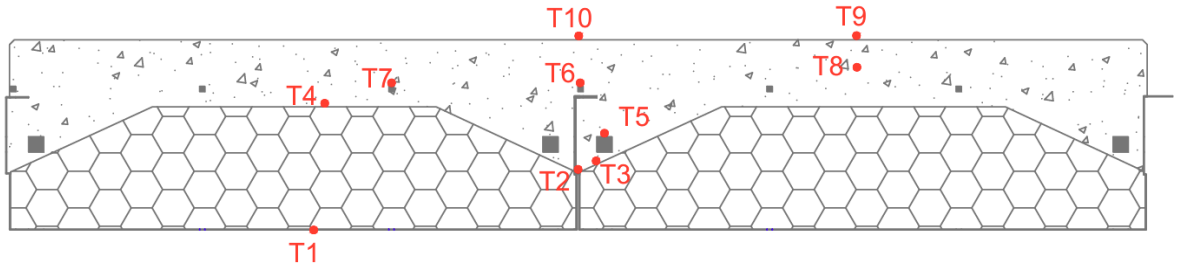

Figure 14 – Ten thermal measurement points.

The ten temperature measuring points are located: T1 on the lower flange, T2 on the web flange, T3 and T4 on the interface between the concrete and rock wool, T5 on the reinforcement rebar, T6 and T7 in the longitudinal reinforcements of the welded

mesh, T8 in the middle height of the concrete and T9 and T10 on the unexposed side of the concrete.

4.4. Average Temperature of Slabs

This section presents a detailed analysis of the results of fire tests carried out at 10 different measurement points. The computational tests were conducted to evaluate the performance of composite slabs with steel deck and mineral wool in fire situations, to validate the computational model developed to predict the behaviour during such events. The analysis includes a comparison between the experimental results and the computer model results, highlighting the difference by calculating the root mean square error.

The graphs in the following figures show the results of the 120-minute fire tests for each of the 10 measurement points. These points were strategically chosen to represent different areas of fire exposure and capture a variety of temperature points in evolution.

The temperature measurement point T1 is located on the lower flange. Figure 15 shows a comparison between the temperatures obtained by the experimental tests and the temperature obtained in the study by X. Duponchel (2006) through the model developed in the SAFIR software and also the temperature obtained by the computational model proposed in this work created by using ANSYS.

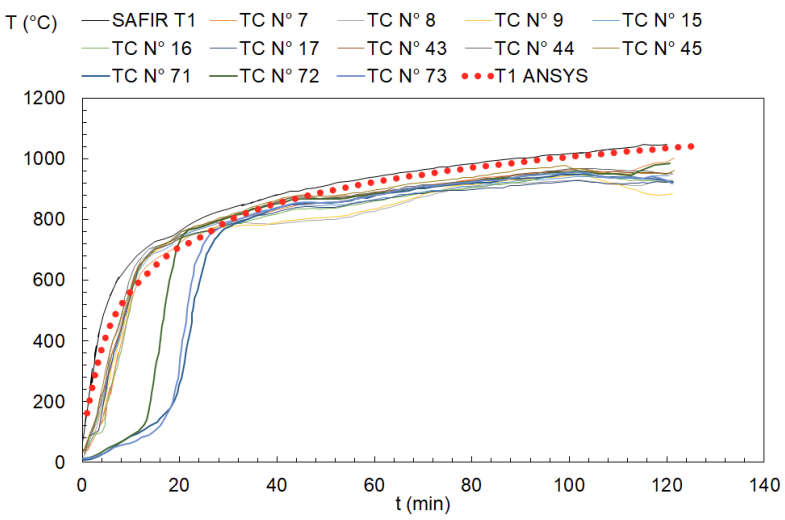

Figure 15 – Comparison of the temperature in T1 obtained by ANSYS with experimental tests.

The temperature measurement point T2 is located on the web flange. Figure 16 shows a comparison between the temperatures obtained by the experimental tests and the temperature obtained in the study by X. Duponchel (2006) through the model developed in the SAFIR software and also the temperature obtained by the computational model proposed in this work created by using ANSYS. The calculation made with ANSYS is near the measurements and the other numerical prediction by SAFIR.

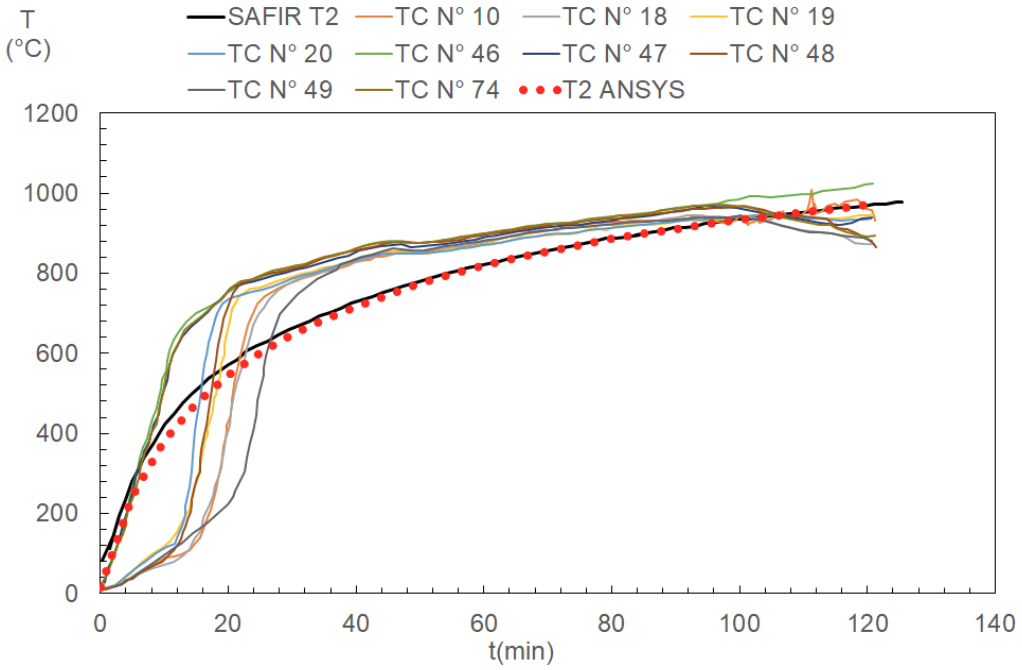

Figure 16 – Comparison of the temperature in T2 obtained by ANSYS with experimental tests.

The temperature measurement point T3 and T4 is located on the interface of concrete and rockwool. Figure 17 shows a comparison between the temperatures obtained by the experimental tests and the temperature obtained in the study by X. Duponchel (2006) through the model developed in the SAFIR software and also the temperature obtained by the computational model proposed in this work created by using ANSYS.

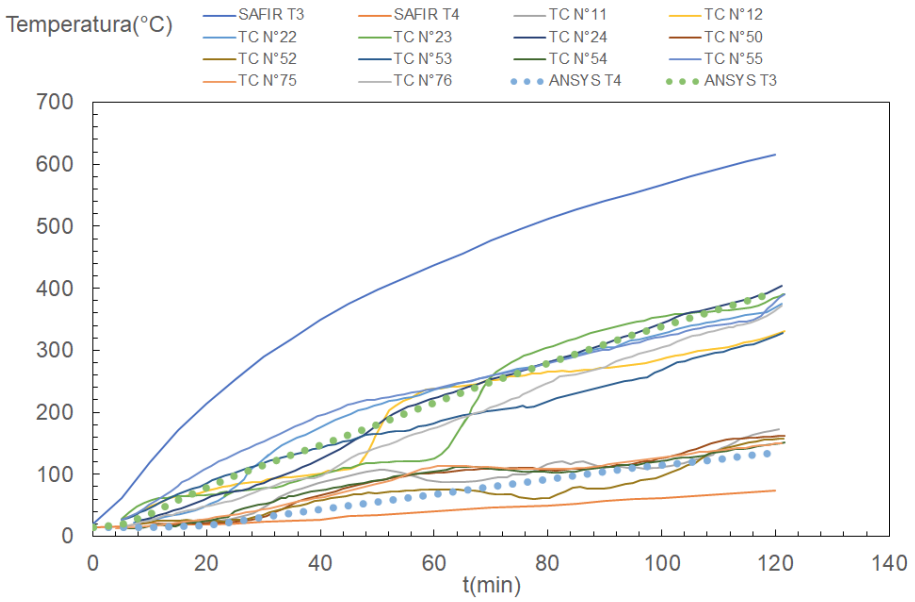

Figure 17 – Comparison of the temperature in T3 and T4 obtained by ANSYS with experimental tests.

The temperature measurement point T5 is located on the reinforcement rebar. Figure 18 shows a comparison between the temperatures obtained by the experimental tests and the temperature obtained in the study by X. Duponchel (2006) through the model developed in the SAFIR software and also the temperature obtained by the computational model proposed in this work created by using ANSYS. The ANSYS result is closer to the experimental measurements than the results obtained by SAFIR.

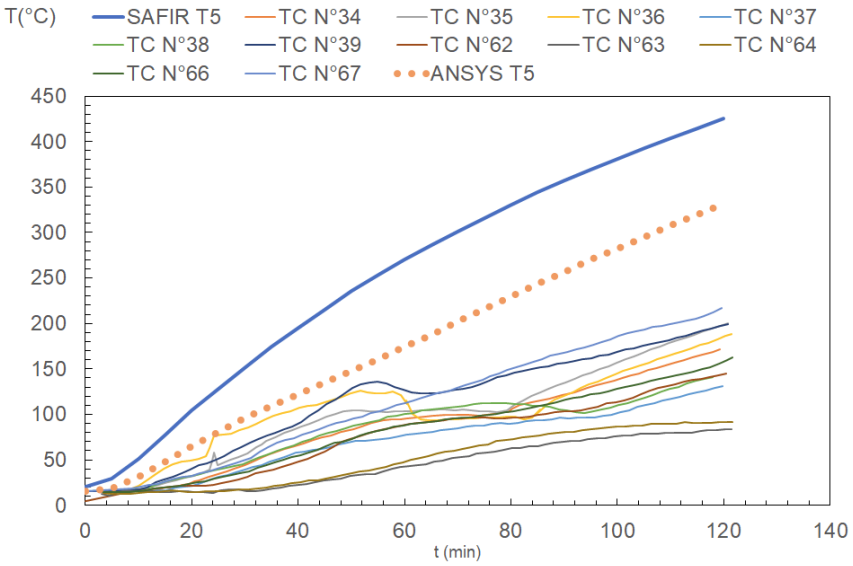

Figure 18 – Comparison of the temperature in T5 obtained by ANSYS with experimental tests.

The temperature measurement points T6 and T7 are located on the longitudinal reinforcements, but with different relative positions. Figure 19 shows a comparison between the temperatures obtained by the experimental tests and the temperature obtained in the study by X. Duponchel (2006) through the model developed in the SAFIR software and also the temperature obtained by the computational model proposed in this work created by using ANSYS.

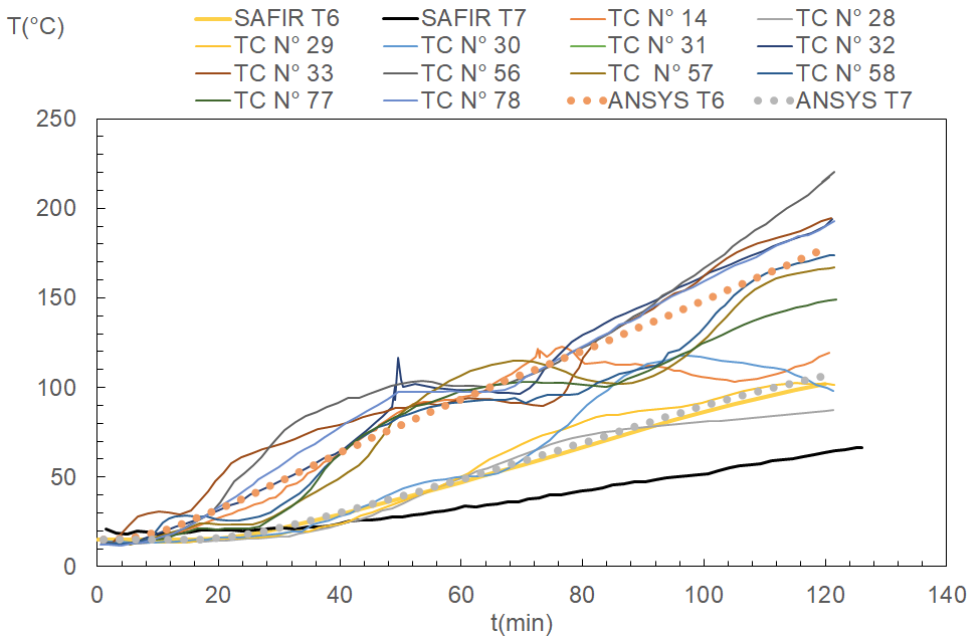

Figure 19 – Comparison of the temperature in T6 and T7 obtained by ANSYS with experimental tests.

The thermal measurement point T8 is located at the middle height of the concrete. Figure 20 shows a comparison between the temperatures obtained by the experimental tests and the temperature obtained in the study by X. Duponchel (2006) through the model developed in the SAFIR software and also the temperature obtained by the computational model proposed in this work by using ANSYS.

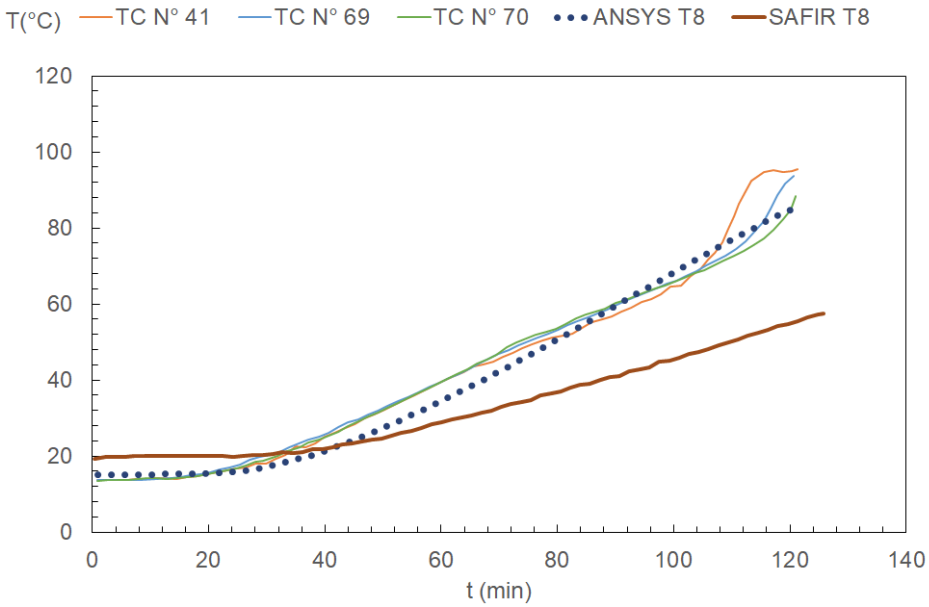

Figure 20 – Comparison of the temperature in T8 obtained by ANSYS with experimental tests.

The temperature measurement points T9 and T10 are located on the unexposed side of the concrete. Figure 21 compares the temperatures obtained by the experimental tests and the temperature obtained in the study by X. Duponchel (2006) through the model developed in the SAFIR software and the temperature obtained by the computational model proposed in this work created by ANSYS.

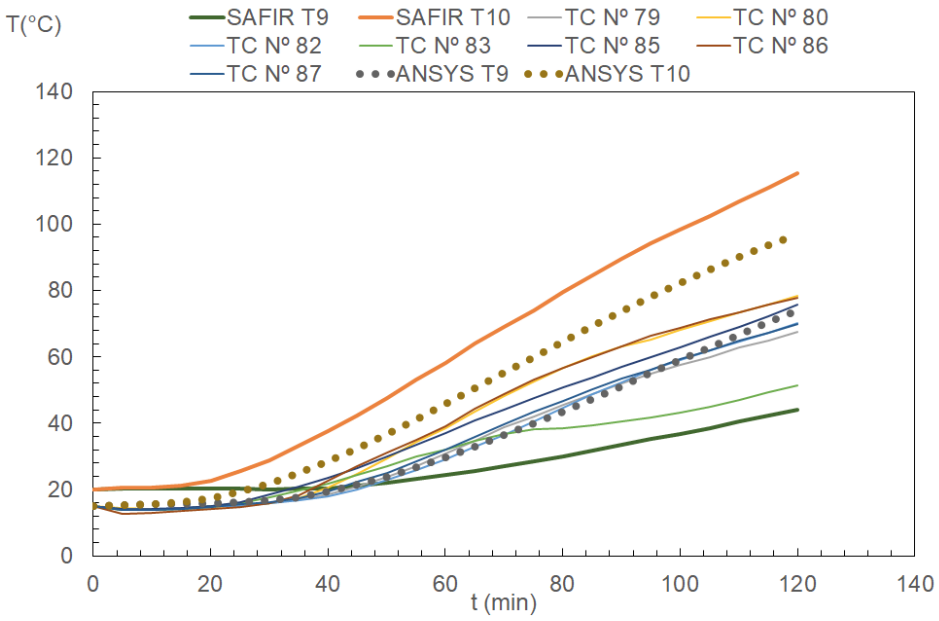

Figure 21 – Comparison of the temperature in T9 and T10 obtained by ANSYS with experimental tests.

The validation of numerical model through comparison with experimental data requires the use of statistical metrics capable of quantifying the degree of agreement between simulated results and measured values. In this context, the Root Mean Square Error (RMSE) is adopted as one of the main performance indicators. The RMSE is calculated, as shown in Equation 14, from the square root of the mean of the squared differences between the values predicted by the model and those observed experimentally, expressing the average magnitude of the error in absolute units of the analysed variable. The RMSE retains the same unit as the variable under analysis, in this case, temperature in (ºC).

$$RMSE = \sqrt{\frac{1}{n}\sum_{i=1}^{n} (T_i^{modelo} - T_i^{exp})^2} \quad (14)$$

Where:

- T_i^{model} are the values estimated by the computational model;
- T_i^{exp} are the values obtained experimentally;
- n is the total number of observations.

In studies such as that by Kodur & Dwaikat (2008), the validation of numerical models is performed through direct comparison with experimental data, considering discrepancies below 10–15% in key variables (temperature, deflection, failure time) to be acceptable. In the context of this work, RMSE values below 10% of the range of the observed data are considered adequate to ensure model reliability, in accordance with established practices in the structural engineering literature under fire conditions (Willmott et al., 2005; EN 1992-1-2:2004). For the analyses developed in this section, the RMSE values obtained are presented in Table 2, and they can also be compared to the tolerance of the temperature used in the furnace tests, according to EN 1363-1 (CEN, 2020). According to this standard, at any time after the first 10 min of the test, the temperature recorded by any thermocouple in the furnace shall not differ from the corresponding temperature of the standard temperature curve by more than 100 [K].

Table 2 – RMSE values for each T point analysed.

T Point	RMSE
T1	86,74
T2	84.17
T3	14,98
T4	20,61
T5	105,05
T6	23,86
T7	27,36
T8	4,18
T9	2,60
T10	18,30

Most of the controlling points are below 100 [K] with the exception of point T5.

4.5. Calculation of Sagging Moment

The bending moment, according to Eurocode, is one of the main parameters in structural design, especially in beams and slabs. This moment results from the forces applied to the structure, causing bending that leads to the distribution of internal stresses along the element.

In the context of Eurocode 2 (EN 1992-1-1) and Eurocode 4 (EN 1994-1-1), the bending moment is treated as a force that induces compression in one part of the cross-section of the element (usually at the top of a slab under sagging conditions) and tension in the other part (at the bottom). Eurocode establishes methods for calculating the resistance to the bending moment, taking into account the geometry of the section, the material strength (steel and concrete), and the loading conditions.

In design situations, the bending moment must be compared with the bending resistance of the section, which is determined by the interaction between the materials and the effective section in question. The specific equations and standards in Eurocode provide guidance for verifying the safety and adequacy of the section under applied loads, ensuring that the stresses do not exceed the allowable limits for the materials in use.

Eurocode also discusses the importance of considering bending moments under different limit states, including the ultimate limit state and the serviceability limit state, to ensure that the structure not only supports the loads but also remains functional and safe over time.

To calculate the bending moment, the first step is determining the neutral axis in composite steel and concrete sections, as described in Eurocode 4 (EN 1994-1-1) and represented by Equation 15. This is done within the framework of balancing the tensile and compressive forces between the two materials, ensuring that the composite section can withstand the applied loads. The neutral axis is determined by ensuring that the sum of compressive forces in the concrete equals the sum of tensile forces in the steel, considering the characteristic strength of each material and the corresponding areas of the components involved.

$$\sum_{i=1}^{n} A_i K_{y,\theta,i} \left(\frac{f_{y,i}}{\gamma_{M,fi,a}}\right) + \alpha_{slab} \sum_{j=1}^{n} A_j K_{c,\theta,j} \left(\frac{f_{y,j}}{\gamma_{M,fi,a}}\right) = 0 \quad (15)$$

The first term denotes the contribution of the steel components. Here, A_k represents the area of the cross-section of the i-th steel component, while $k_{y,\theta,i}$ is a geometrical factor that considers the position of the i-th component in relation to the neutral axis and the angle of loading. The yield strength of the i-th steel component is denoted by $f_{y,i}$, indicating the material's capacity to withstand yielding under applied loads. The term $\gamma_{M,f,a}$ is a partial safety factor for the steel material, enhancing design safety by reducing the yield strength in calculations.

The second term relates to the concrete component. The factor α_{slab} adjusts the contribution of the concrete slab in the composite action, reflecting its interaction with the steel. The area of the cross-section of the j-th concrete component is represented by A_j, while $k_{c,\theta,j}$ is a geometrical factor that relates the position of the j-th concrete component to the neutral axis. The compressive strength of the j-th concrete component is indicated by $f_{c,j}$, and $\gamma_{M,f,\mathrm{c}}$ is a partial safety factor for the concrete material, ensuring safety by reducing the compressive strength in design calculations.

The design moment resistance $M_{fi,t,Rd}$ may be determined from the equation 16.

$$M_{fi,t,Rd} \sum_{i=1}^{n} A_i Z_i K_{y,\theta,i} \left(\frac{f_{y,i}}{\gamma_{M,fi,a}}\right) + \alpha_{slab} A_j z_j K_{c,\theta,j} \left(\frac{f_{y,j}}{\gamma_{M,fi,a}}\right) \quad (16)$$

Where Z_i , z_j are the distance from the plastic neutral axis to the centroid of the elemental area A_i or $A_{j\text{j}}$. After performing all the calculations, the resistant bending moment was obtained after each 30-minute cycle, as shown in the following Table 5.

Table 3 – Resistant Bending Moment.

Time	Moment Resistance (N x m)
0 minutes	121957.25
30 minutes	63193.64
60 minutes	58923.12
90 minutes	56230.80
120 minutes	47065.24

5. PARAMETRIC ANALYSIS

Parametric analyses of slabs subjected to fire constitute an essential approach in structural design, particularly when seeking to understand the thermal and structural behaviour of these elements under fire conditions. This type of analysis considers a range of parameters that influence the slab's response to high temperatures, such as material strength, cross-sectional geometry, heating rate, and other relevant factors.

Parametric studies aim to assess how different variables affect the performance of slabs when exposed to fire, allowing for the optimisation of the design to ensure structural safety. These analyses typically involve advanced computational simulations, considering complex thermal and structural models to predict the slab's behaviour over time during a fire.

The primary goal of parametric analyses is to provide valuable insights to engineers and designers, enabling them to make informed decisions about fire protection measures, material selection, and design strategies that ensure the structural integrity of slabs in emergencies. Thus, the parametric approach plays a crucial role in finding effective and secure solutions for structures exposed to extreme temperature conditions.

The parametric analysis of this work addressed a comprehensive exploration of various critical factors to understand their impact on the structural and thermal behaviour of slabs subjected to fire. Figure 22 presents the components of the parametric analysis performed. Specifically, the following parameters were varied:

- Concrete Height (h): Three different concrete heights – 60 [mm], 90 [mm], and 120 [mm] - were examined to observe how the thickness of the concrete section influences the response to fire conditions.
- Rebar Diameter (d): Two rebar diameters were investigated – 12 [mm] and 16 [mm] - to evaluate the effect of reinforcement size on the structural performance of the slabs during exposure to fire.
- Thermal Insulation Height (h_insulation): The height of thermal insulation, using rockwool, varied across three levels – 130 [mm], 98 [mm], and 60 [mm] - to assess its impact on heat transfer and the preservation of structural integrity of the slabs under fire.

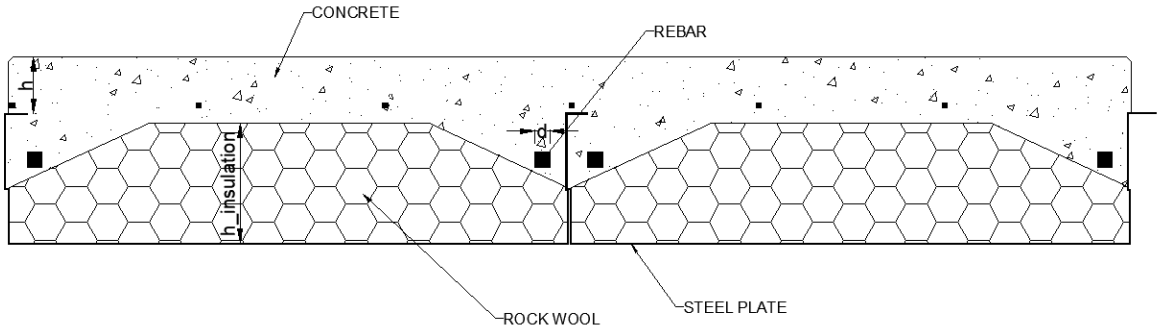

Figure 22 – Components of parametric analysis.

This systematic exploration resulted in a total of 18 different models, each representing a unique combination of the aforementioned parameters. These models were crucial for examining how variations in concrete thickness, rebar diameter, and insulation height contribute to temperature fluctuations during a fire event.

In addition to these parameters, variations in the yield strength of the steel were also introduced, ranging from 320 [MPa] to 280 [MPa]. However, it is important to note that these modifications specifically influenced the calculation of moment resistance, representing a key aspect in evaluating the structural capacity of the slabs.

Through this comprehensive parametric analysis, valuable insights were gained into the intricate interplay of these variables, enabling a nuanced understanding of their collective impact on the performance of slabs under fire conditions.

Below, Table 4 and Table 5 are presented, with Table 4 illustrating the parameters varied in the parametric analysis, while Table 5 showcases the models derived from the parametric study. In Table 4, parameters such as concrete height, rebar diameter, and thermal insulation height, which underwent variations during the study, are highlighted. Table 5 provides a detailed overview of the diverse models generated from the parametric analysis, offering a comprehensive view of the different combinations of these elements and their influences on the outcomes. These tables have been crafted to facilitate the understanding and reference of the conclusions drawn from the parametric analysis.

Table 4 – Parametric Analyses.

Concrete Height (mm)	Rebar Diameter (mm)	Rock Wool Height (mm)	Yield Stress Of Steel (MPa)
60, 90, 120	16, 12	130, 98, 60	320, 280

Table 5 – Models obtained from parametric analysis.

Models	Concrete Height (mm)	Rebar Diameter (mm)	Rock Wool Height (mm)	Yield Stress Of Steel (MPa)
1	60	16	130	320
2	90	16	130	320
3	120	16	130	320
4	60	12	130	320
5	90	12	130	320
6	120	12	130	320
7	60	16	98	320
8	90	16	98	320
9	120	16	98	320
10	60	12	98	320
11	90	12	98	320
12	120	12	98	320
13	60	16	60	320
14	90	16	60	320
15	120	16	60	320
16	60	12	60	320
17	90	12	60	320
18	120	12	60	320
19	60	16	130	280
20	90	16	130	280
21	120	16	130	280
22	60	12	130	280
23	90	12	130	280
24	120	12	130	280
25	60	16	98	280
26	90	16	98	280
27	120	16	98	280
28	60	12	98	280
29	90	12	98	280
30	120	12	98	280
31	60	16	60	280
32	90	16	60	280
33	120	16	60	280
34	60	12	60	280
35	90	12	60	280
36	120	12	60	280

The following six images visually depict variations among different images resulting from the manipulation of key parameters. Figure 23 (Model 1) features a concrete height of 60 [mm], a rebar diameter of 16 [mm], and rock wool insulation with a height of 130 [mm].

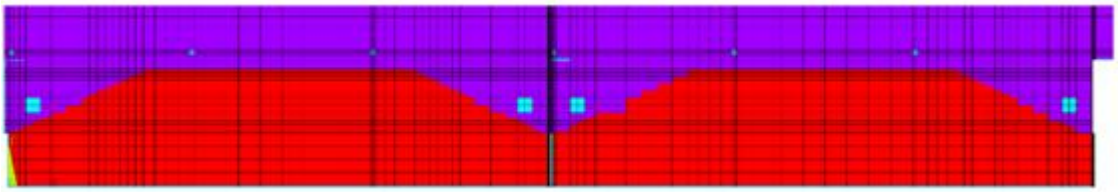

Figure 23 – Model 1: concrete height 60mm, rebar diameter 16mm, rockwool height 130mm.

In Figure 24 (Model 2), the concrete height increases to 90 [mm] while maintaining the same rebar diameter and insulation height.

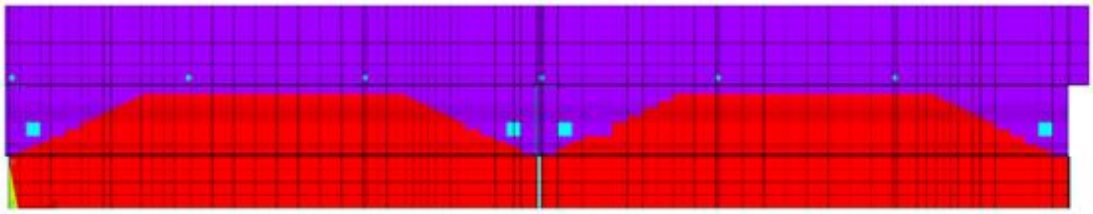

Figure 24 – Model 2: concrete height 90mm, rebar diameter 16mm, rockwool height 130mm.

Now, in Figure 25 (Model 3) exhibits a concrete height of 120 [mm], still with a rebar diameter of 16 mm and rock wool insulation measuring 130 [mm] in height.

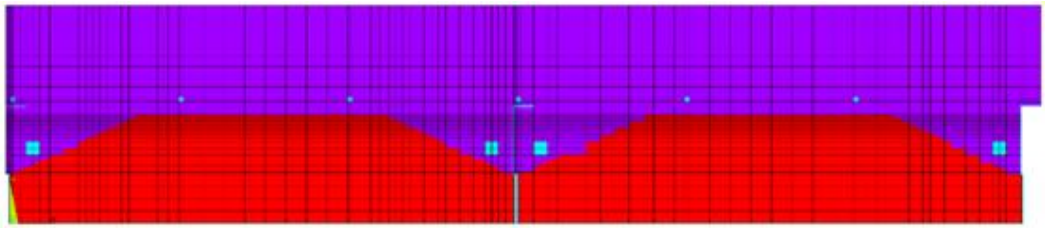

Figure 25 – Model 3: concrete height 120mm, rebar diameter 16mm,rockwool height 130mm.

In Figure 26 (Model 5), the concrete height is set at 90 [mm], but with a reduced rebar diameter of 12 [mm], while maintaining the insulation height at 130 [mm].

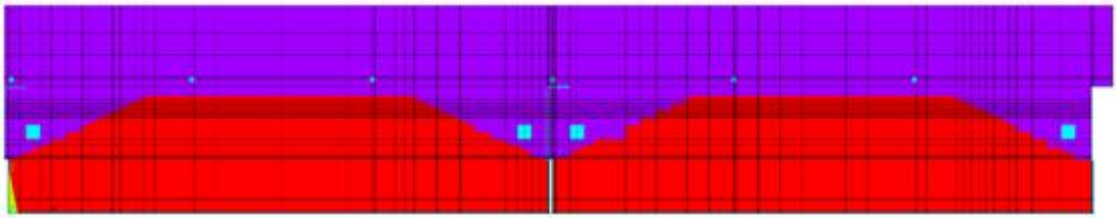

Figure 26 – Model 5: concrete height 90mm, rebar diameter 12mm, rockwool height 130mm.

For its time, Image 5 (Model 11) introduces a change in insulation height to 98 [mm] while keeping the concrete height at 90 [mm] and the rebar diameter at 12 [mm].

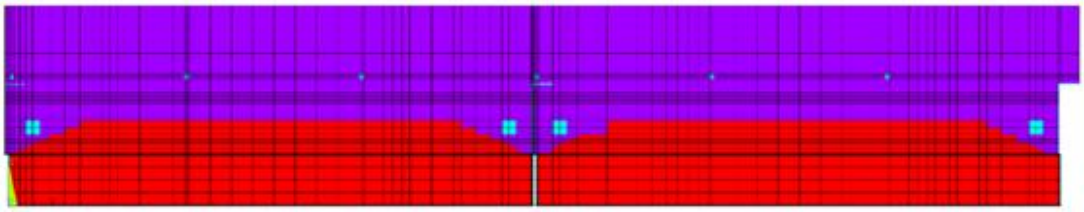

Figure 27 – Model 11: concrete height 90mm, rebar diameter 12mm, rockwool height 98mm.

Lastly, Figure 28 (Model 15) showcases a concrete height of 120 [mm], a rebar diameter of 16 [mm], and a reduced rock wool insulation height of 60 [mm].

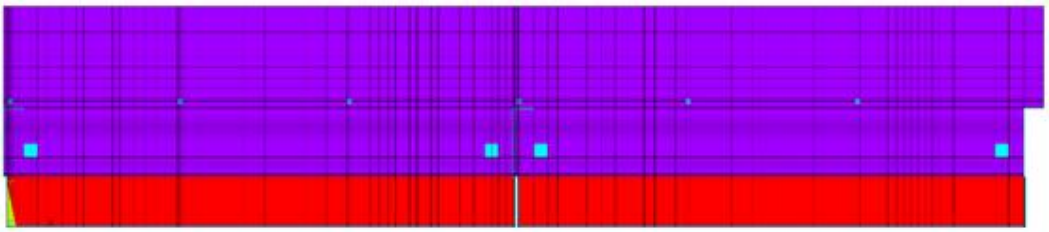

Figure 28 – Model 15: concrete height 120mm, rebar diameter 16mm, rockwool height 60mm.

These images provide a visual insight into the parameter effects of altering concrete height, rebar diameter, and insulation dimensions, contributing to a

comprehensive understanding of the diverse outcomes derived from the parametric analysis.

5.1. Average temperature on each component

The average temperature for each component of the slab was obtained through the numerical model, duly validated to ensure the accuracy of predictions. This two-dimensional model meticulously considered the different components of the slab.

Model validation is a crucial step to ensure that numerical predictions reliably correspond to the actual behaviour of the structure. Experimental data, when available, were used to compare and adjust the model, ensuring that real temperature conditions were accurately represented.

Throughout the simulation, thermal properties of materials, temporal variations in environmental conditions, and other relevant factors were taken into account. Heat transfer between slab components was modelled.

The numerical analysis not only allowed the determination of the average temperature for each slab element but also provided a detailed visualisation of thermal patterns over time and in different regions of the structure. The use of finite elements and high-quality meshes contributed to an accurate representation of local behaviour, while continuous model validation strengthened the reliability of the results.

Temperature data were collected from ANSYS at strategic points to calculate the average temperature for each specific element of the slab. For the lower flange, measurements were taken at 12 distinct points, providing a detailed analysis of this region. Similarly, readings were conducted at 8 points on web 1, 4 points on web 2, 3 points on the upper flange, and 8 points on the rebar.

This approach of collecting data at multiple points not only facilitates the determination of averages but also offers a more comprehensive understanding of temperature variations across different components of the slab. Each measurement point significantly contributed to the analysis of thermal gradients in specific elements, providing a more complete and refined insight into the thermal behaviour of the structure when exposed to fire. This strategic approach, utilising a substantial number of collection points, enables a more precise assessment of the impact of thermal variations on the integrity of the slab, allowing decision-making based on concrete data.

The temperature averages for each element were calculated at specific time intervals during the analysis in ANSYS. Data were collected at the 30, 60, 90, and 120-minute marks, enabling a detailed assessment of thermal evolution throughout the exposure period. This temporal approach provides a dynamic understanding of temperature variations in each slab component, allowing for the identification of patterns, trends, and potential critical points over the course of the process.

Here is presented the detailed temperature gradient profile of the slab COFRADAL 200, corresponding to Model 1 in Table 5. The thermal evolution of the slab can be observed at 30 minutes, as illustrated in Figure 29, followed by a more in-depth analysis at 60 minutes in Figure 30. At 90 minutes, the exploration of the thermal gradient is depicted in Figure 31, culminating in a comprehensive understanding of the test at 120 minutes, as evidenced in Figure 32.

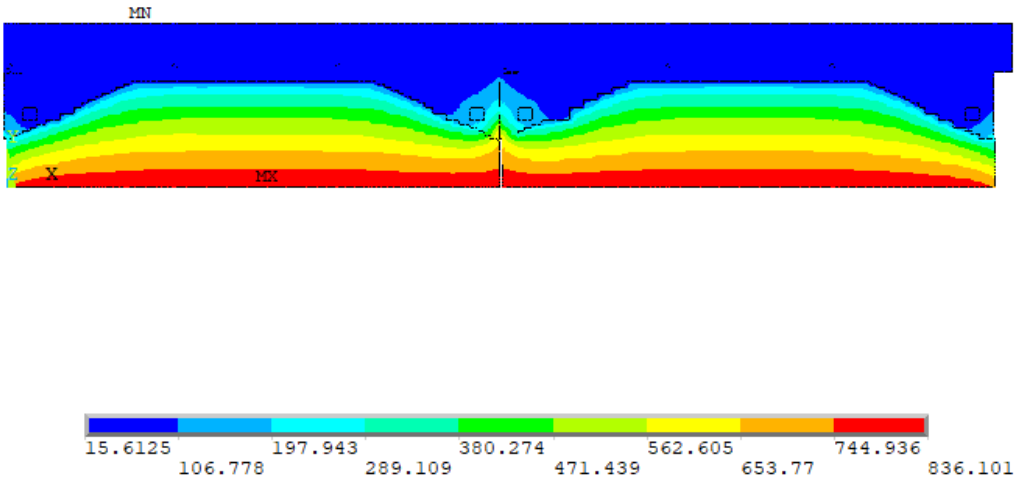

Figure 29 – Model 1: Temperature on the slab at 30 minutes.

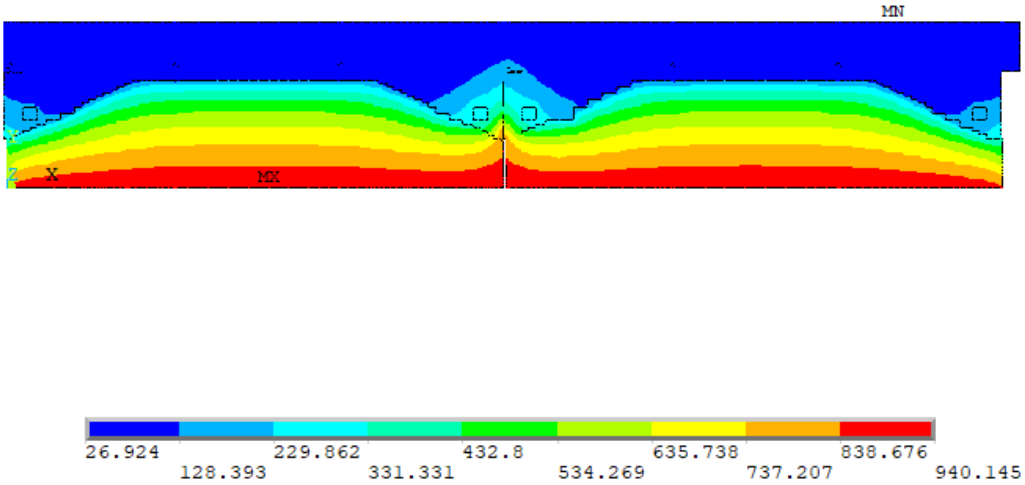

Figure 30 – Model 1: Temperature on the slab at 60 minutes.

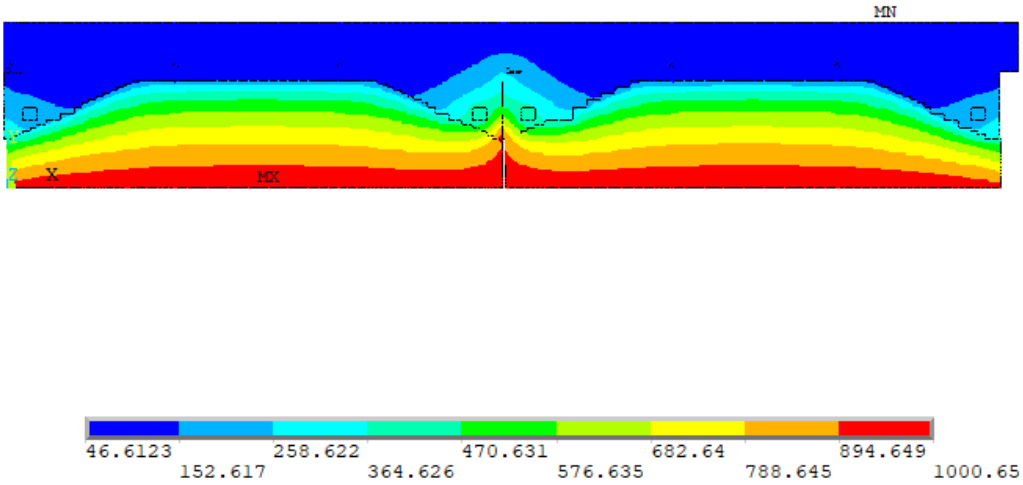

Figure 31 – Model 1: Temperature on the slab at 90 minutes.

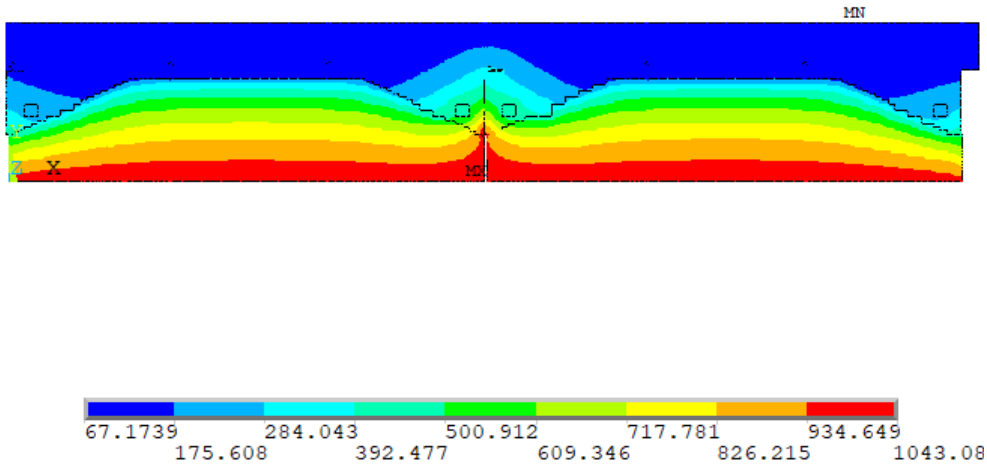

Figure 32 – Model 1: Temperature on the slab at 120 minutes.

The analysis presented for Model 1 in Table 5 was replicated for the other 18 models listed in the same table, encompassing a wide range of scenarios. This procedure facilitated a comprehensive investigation, taking into account significant variations in the modelled conditions and parameters. The results obtained from each simulation were collected at intervals of 30, 60, 90, and 120 minutes, ensuring comprehensive coverage over time. Following the completion of the numerical simulation and the thorough analysis of the obtained data, the results were organised and presented in the tables below, consolidating a holistic view of the thermal behaviours observed in the different models of the parametric analysis. Table 6 shows the results of the temperatures measured after applying the ISO 834 fire curve for 30 minutes.

Table 6 – Average temperature in each component after 30 minutes.

MODEL	AVERAGE OF LOWER FLANGE (°C)	AVERAGE OF WEB 1 (°C)	AVERAGE OF WEB 2 (°C)	AVERAGE OF UPPER FLANGE (°C)	AVERAGE OF REBAR (°C)
1	829.8	725.0	291.6	87.3	158.1
2	824.2	726.2	298.5	86.8	157.8
3	826.6	719.8	301.1	86.2	158.1
4	827.8	725.1	304.0	86.1	158.1
5	825.3	708.1	315.8	86.2	158.1
6	818.2	735.2	306.1	85.6	159.2
7	821.4	725.5	296.3	86.5	158.1
8	818.8	735.1	289.4	85.9	158.4
9	809.7	721.1	300.1	86.7	158.4
10	812.3	715.8	276.6	86.6	158.4
11	818.8	716.1	333.5	86.1	158.4
12	818.2	718.7	316.3	87.0	159.5
13	810.9	708.4	300.9	82.4	139.6
14	824.2	726.2	298.5	86.8	157.8
15	826.6	719.8	301.1	86.2	158.1
16	822.8	715.0	281.2	82.9	139.2
17	818.2	708.5	285.3	82.5	139.6
18	814.7	711.5	302.1	83.2	139.2

Table 7 shows the results of the temperatures measured after applying the ISO 834 fire curve for 60 minutes.

Table 7 – Average temperature in each component after 60 minutes.

Model	Average of Lower Flange (°C)	Average of Web 1 (°C)	Average of Web 2 (°C)	Average of Upper Flange (°C)	Average of Rebar (°C)
1	936,2	868,5	427,2	168,1	295,6
2	931,5	869,2	432,0	165,8	294,9
3	934,3	864,6	433,7	164,6	295,3
4	935,2	868,7	437,1	166,1	295,6
5	933,3	857,3	452,0	164,8	295,3
6	927,1	875,2	441,5	163,9	299,9
7	929,3	867,7	427,5	165,9	292,9
8	928,5	874,1	418,6	163,7	293,8
9	921,1	865,2	432,1	164,7	293,8
10	923,2	861,2	408,6	166,3	294,1
11	928,5	861,7	471,4	164,1	293,8
12	927,6	864,5	452,7	166,2	300,4
13	877,7	849,5	437,9	154,2	295,6
14	931,5	869,2	432,0	165,8	294,9
15	934,3	864,6	433,7	164,6	295,3
16	929,8	854,3	406,2	155,0	258,4
17	925,7	849,6	408,9	153,0	258,6
18	923,9	852,8	428,8	153,4	259,2

Table 8 shows the results of the temperatures measured after applying the ISO 834 fire curve for 90 minutes.

Table 8 – Average temperature in each component after 90 minutes.

Model	Average of Lower Flange (°C)	Average of Web 1 (°C)	Average of Web 2 (°C)	Average of Upper Flange (°C)	Average of Rebar (°C)
1	997,6	944,0	520,2	243,8	398,1
2	993,2	944,6	521,5	238,7	396,3
3	996,2	940,6	522,3	236,6	396,4
4	996,9	944,4	527,5	241,7	398,1
5	995,4	935,9	542,3	237,5	396,6
6	989,6	948,5	530,1	235,0	400,7
7	991,8	942,3	516,0	239,5	391,7
8	991,3	947,1	505,4	234,8	392,5
9	984,7	940,8	519,6	235,3	392,3

10	986,7	937,3	499,9	240,3	393,9
11	991,3	938,0	560,9	235,2	392,5
12	990,5	940,7	541,5	237,7	401,3
13	946,9	927,8	525,6	222,0	398,1
14	993,2	944,6	521,5	238,7	396,3
15	996,2	940,6	522,3	236,6	396,4
16	991,7	930,6	493,2	223,0	351,0
17	988,0	926,9	494,1	218,4	350,4
18	986,7	929,7	513,3	217,4	350,5

Table 9 shows the results of the temperatures measured after applying the ISO 834 fire curve for 120 minutes.

Table 9 – Average temperature in each component after 120 minutes.

MODEL	AVERAGE OF LOWER FLANGE (°C)	AVERAGE OF WEB 1 (°C)	AVERAGE OF WEB 2 (°C)	AVERAGE OF UPPER FLANGE (°C)	AVERAGE OF REBAR (°C)
1	1040,8	995,3	590,1	307,4	479,0
2	1036,5	995,6	588,5	299,8	475,6
3	1039,5	992,0	588,3	296,4	475,2
4	1040,2	995,7	595,6	305,2	479,0
5	1038,9	988,8	609,7	298,6	475,9
6	1033,5	998,5	595,7	293,8	478,5
7	1035,4	992,6	581,9	300,4	468,8
8	1035,2	996,7	570,1	293,8	468,9
9	1029,2	991,8	584,3	293,3	468,2
10	1031,0	988,7	568,2	301,8	471,9
11	1035,2	989,4	626,9	294,3	468,9
12	1034,6	992,2	607,2	296,9	479,2
13	995,6	980,9	591,5	279,9	479,0
14	1036,5	995,6	588,5	299,8	475,6
15	1039,5	992,0	588,3	296,4	475,2
16	1035,3	982,7	559,0	281,0	425,8
17	1031,9	979,5	558,2	274,1	424,0
18	1030,6	981,5	576,1	271,3	423,3

After the previously discussed parametric analyses, it was noted that varying the height of the concrete did not result in a significant variation in the temperature of the slab components after 120 minutes of fire exposure. However, in the calculation of the flexural moment to be presented, a difference was observed. This discrepancy

underscores the importance of considering not only immediate thermal effects but also long-term structural consequences, especially in situations of exposure to high temperatures.

When varying the diameter of the steel bar, no significant influence on the temperature of the slab components after 120 minutes of fire was observed. However, in the calculation of the flexural moment to be presented later, a substantial difference was found. This highlights the need for an integrated approach when considering material parameters, ensuring that structural variations are properly addressed in thermal analyses.

In varying the height of the thermal insulation with rock wool, it was observed that the components of the slab above the rock wool experienced a slight decrease in temperature after 120 minutes of fire. However, it is important to note that this variation was relatively small under high-temperature conditions. This analysis emphasises the effectiveness of rock wool as a thermal insulator and its moderate influence on thermal distribution over time.

Considering the variation in the yield strength of the steel plate, no significant change in temperature was identified. However, in the calculation of the flexural moment to be presented later, a relevant influence was observed. This finding highlights the complexity of interactions between the mechanical properties of materials and thermal effects, indicating the importance of a holistic approach in structural and thermal analyses.

5.2. Sagging Moment

The graphs presented in this section are organised into six groups, all structured to account for variations in concrete height (60 mm, 90 mm, and 120 mm) and steel yield stress (280 MPa and 320 MPa). The distinction between the groups lies in the specific combinations of rebar diameter and rockwool thickness, enabling a detailed comparative analysis of the effects of these parameters on the evolution of the sagging moment over time under thermal exposure.

Figure 33 shows the results for a configuration with 12 [mm] diameter rebar and 60 [mm] of rock wool. The initial bending moment values indicate that a greater concrete thickness and higher steel yield strength enhance the slab’s load-bearing capacity before fire exposure. However, thermal degradation occurs rapidly, with a

significant loss of strength within the first 30 minutes – reductions exceeding 55% in some configurations. Beyond this initial phase, the decline in the bending moment continues, but at a less pronounced rate. This suggests that the early stage of fire exposure is the most critical for structural stability.

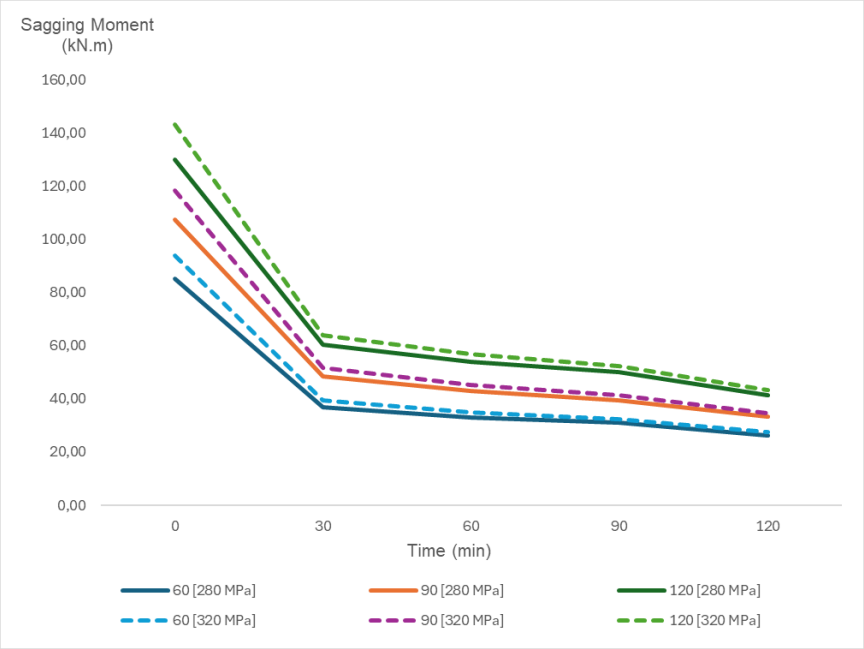

Figure 33 – Sagging Moment Evolution Under Fire: 12 mm Rebar / 60 mm RW.

The analysis of the variation of the strength, as presented in Figure 34 and detailed in Table 10, reinforces this observation by showing that after 120 minutes the structure retains only about 30% of its original strength. Although concrete thickness has a modest influence on the residual capacity, it does not prevent a substantial loss of strength. Additionally, variation in steel yield strength significantly affects the initial bending moments, yet this influence diminishes as the duration of heat exposure increases. These results indicate that with only 60 mm of rock wool insulation, the slab is unable to maintain its structural integrity during prolonged fire exposure, underscoring the need to optimise both thermal protection and structural reinforcement parameters.

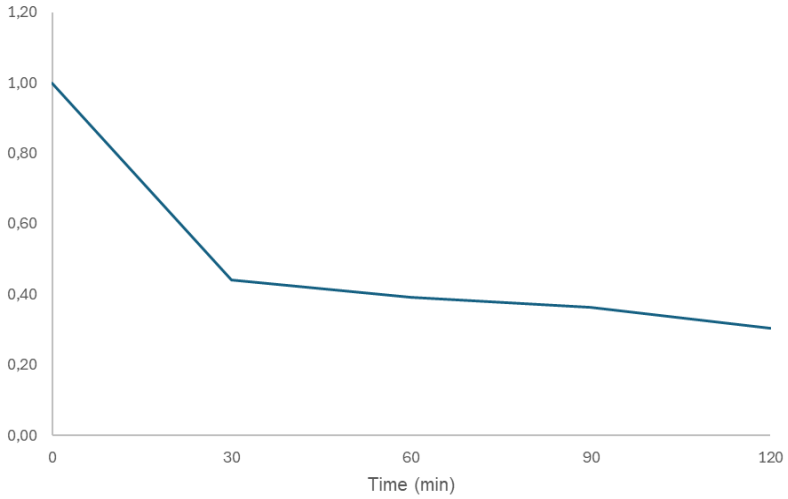

Figure 34 – Residual strength graph: 12 mm Rebar / 60 mm RW.

Table 10 – Bending resistance data: 12 mm Rebar / 60 mm RW.

Classe Aço	**280 MPa**			**320 MPa**			**Variation of the Resistance during fire (average)**
Concrete Height [mm] / **Time [min]**	**60**	**90**	**120**	**60**	**90**	**120**	
0	1,00	1,00	1,00	1,00	1,00	1,00	1,00
30	0,43	0,45	0,46	0,42	0,44	0,45	0,44
60	0,39	0,40	0,42	0,37	0,38	0,40	0,39
90	0,36	0,37	0,38	0,35	0,35	0,37	0,36
120	0,31	0,31	0,32	0,29	0,29	0,30	0,30

Figure 35 presents the results for the configuration with 16-mm rebar and 60 mm of rockwool. Compared to the previous case, there is an overall increase in the initial bending moment, highlighting the positive impact of using a larger rebar diameter on the slab's structural capacity. Nevertheless, the trend of thermal degradation over time persists, with a marked reduction during the first 30 minutes followed by a gradual decline in subsequent intervals. The influence of concrete thickness remains evident, as thicker slabs demonstrate greater fire resistance, although this difference becomes less pronounced after 120 minutes of exposure.

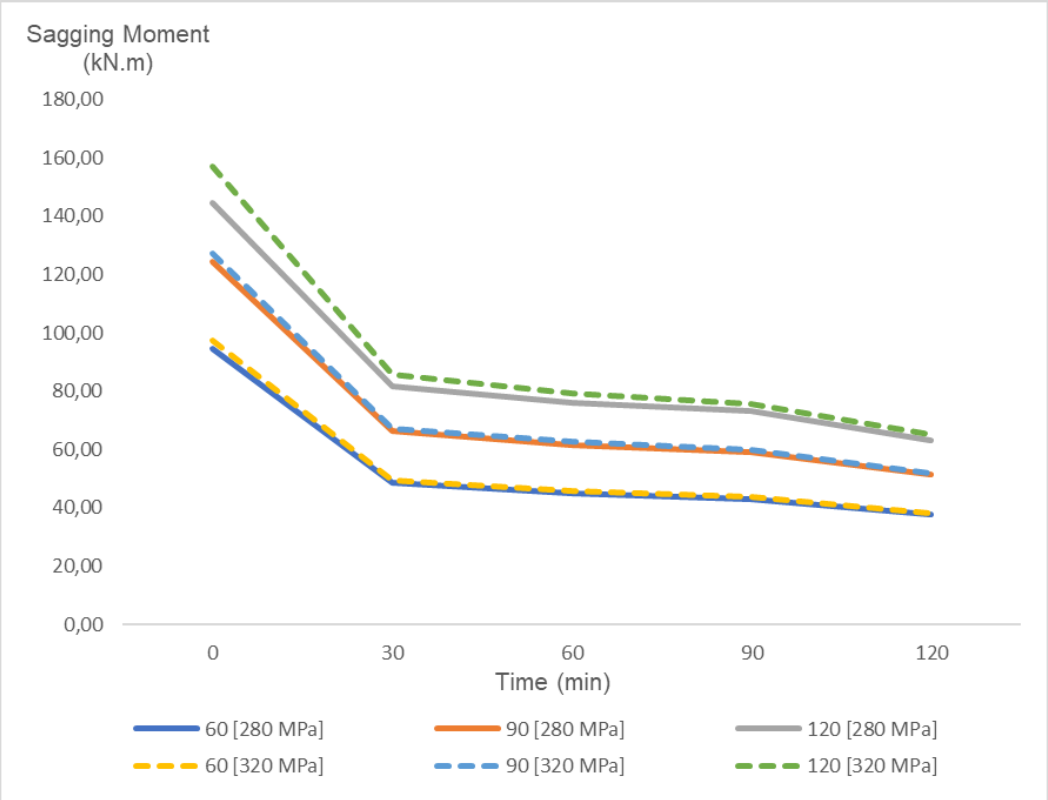

Figure 35 – Sagging Moment Evolution Under Fire: 16 mm Rebar / 60 mm RW.

Subsequently, as shown in Figure 36 and Table 11, the average residual strength is slightly higher than that observed in the previous configuration, maintaining around 40% of the initial strength by the end of the test. The effect of steel yield strength becomes less significant in the later stages of heat exposure, reinforcing the notion that thermal degradation predominantly governs the slab's structural behaviour. Despite the improvements observed with the larger rebar, the protection provided by 60 mm of rock wool is still insufficient to ensure satisfactory structural performance during prolonged fire exposure.

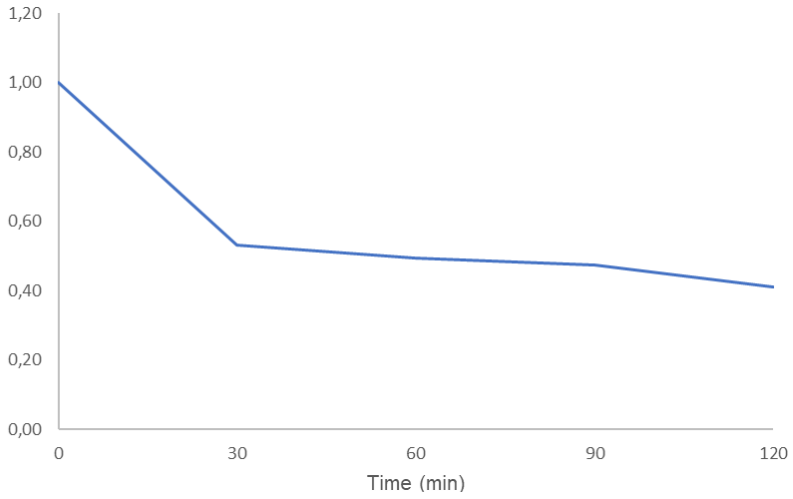

Figure 36 – Residual strength graph: 16 mm Rebar / 60 mm RW.

Table 11 – Bending resistance data: 16 mm Rebar / 60 mm RW.

Classe Aço	**280 MPa**			**320 MPa**			**Variation of the Resistance during fire (average)**
Concrete Height [mm] / **Time [min]**	**60**	**90**	**120**	**60**	**90**	**120**	
0	1,00	1,00	1,00	1,00	1,00	1,00	1,00
30	0,51	0,53	0,56	0,51	0,53	0,54	0,53
60	0,47	0,50	0,53	0,47	0,49	0,50	0,49
90	0,46	0,48	0,51	0,45	0,47	0,48	0,47
120	0,40	0,41	0,44	0,39	0,41	0,41	0,41

In the case of the configuration with 12 [mm] rebar and 98 [mm] of rock wool, as illustrated in Figure 37, the increased thickness of the rock wool positively influences the retention of the bending moment over time, even though the overall trend of thermal degradation remains. Although the strength loss in the first 30 minutes continues to be significant, the bending moment values are slightly higher than those observed with 60 mm of rockwool.

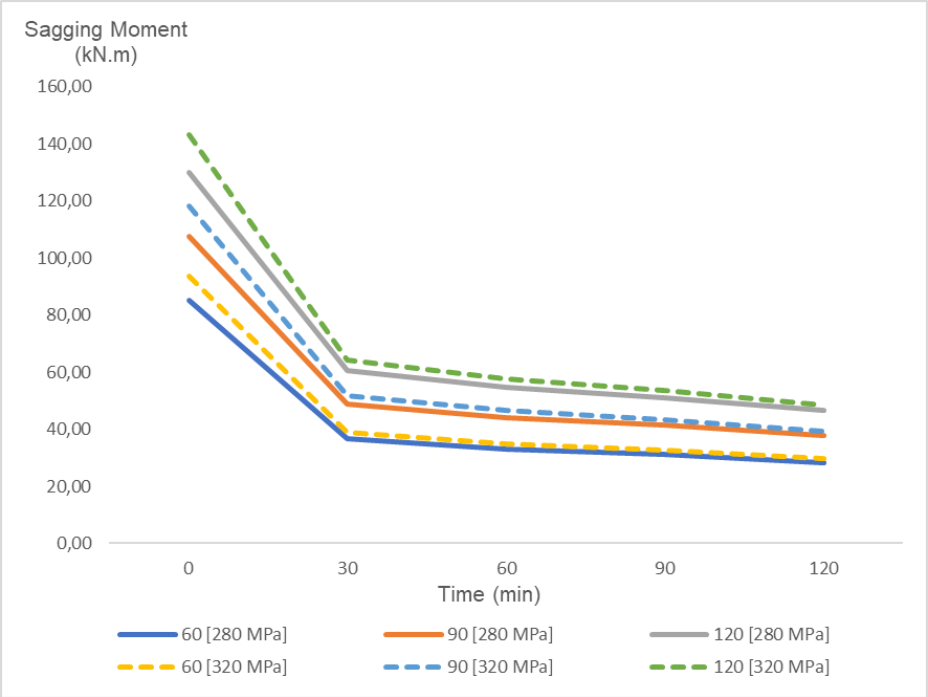

Figure 37 – Sagging Moment Evolution Under Fire: 12 mm Rebar / 98 mm RW.

The average variation of the load-bearing capacity, as depicted in Figure 38 and Table 12, further reflects this effect by exhibiting marginally higher values compared to previous configurations, especially at longer exposure durations. After 120 minutes of fire exposure, the residual strength remains above 34% of the initial capacity, indicating that enhanced thermal insulation improves the slab's structural capacity by delaying the degradation of both concrete and steel. Nonetheless, the significant loss of strength over time highlights the need for additional protection strategies to ensure the slab's integrity under prolonged fire exposure.

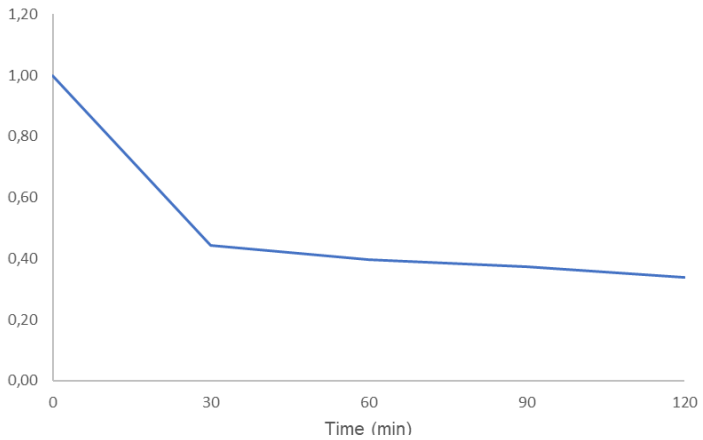

Figure 38 – Residual strength graph: 12 mm Rebar / 98 mm RW.

Table 12 – Bending resistance data: 12 mm Rebar / 98 mm RW.

Classe Aço	280 MPa			320 MPa			Variation of the Resistance during fire (average)
Concrete Height [mm] / Time [min]	60	90	120	60	90	120	
0	1,00	1,00	1,00	1,00	1,00	1,00	1,00
30	0,43	0,45	0,47	0,42	0,44	0,45	0,44
60	0,39	0,41	0,42	0,37	0,39	0,40	0,40
90	0,37	0,39	0,39	0,35	0,37	0,37	0,37
120	0,33	0,35	0,36	0,32	0,33	0,34	0,34

Considering the results presented in Figure 39 for the configuration with 16 [mm] rebar and 98 [mm] of rockwool, it is evident that increasing the rebar diameter continues to enhance the initial strength, while the thicker rockwool contributes to a slower rate of thermal degradation over time. However, the reduction in the bending moment during the first 30 minutes remains significant, with a relative stabilisation in the subsequent intervals. The influence of concrete thickness follows the same pattern observed in earlier stages, with thicker slabs exhibiting superior structural performance.

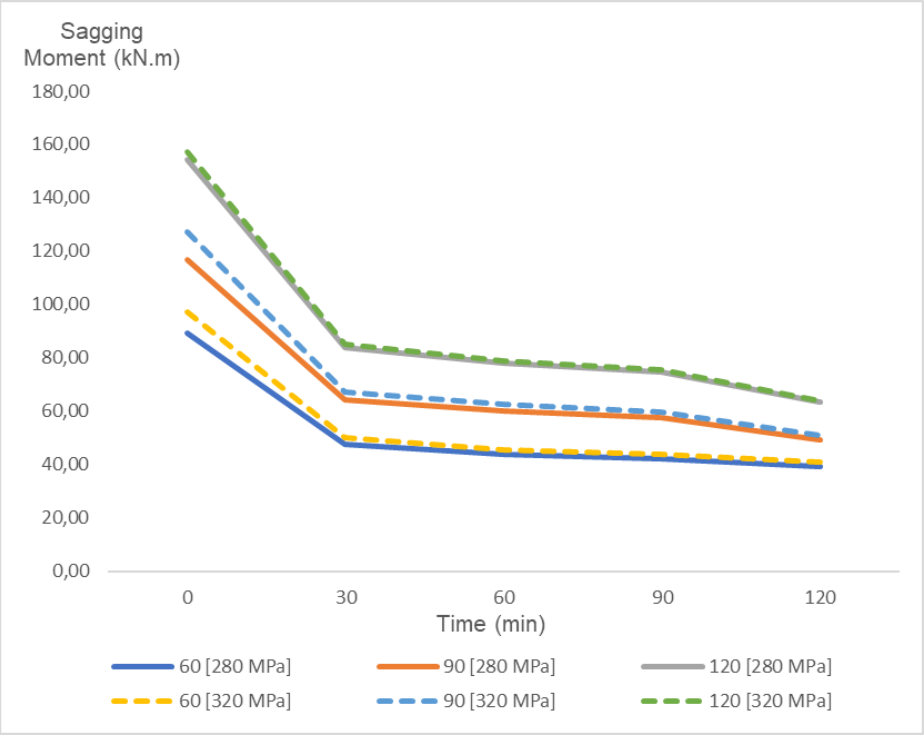

Figure 39 – Sagging Moment Evolution Under Fire: 16 mm Rebar / 98 mm RW.

As shown in Table 13 and Figure 40, the average reduction in the load-bearing capacity after 120 minutes remains above 42%, underscoring the effectiveness of a thicker thermal insulation layer. Although the effect of steel yield strength becomes less pronounced with prolonged exposure, the combination of larger rebar and 98 mm of rock wool results in an overall improvement in retaining structural capacity. This indicates that, although thermal degradation is inevitable, employing more robust thermal insulation in conjunction with adequate steel reinforcement can delay the loss of strength in the slab under prolonged fire scenarios.

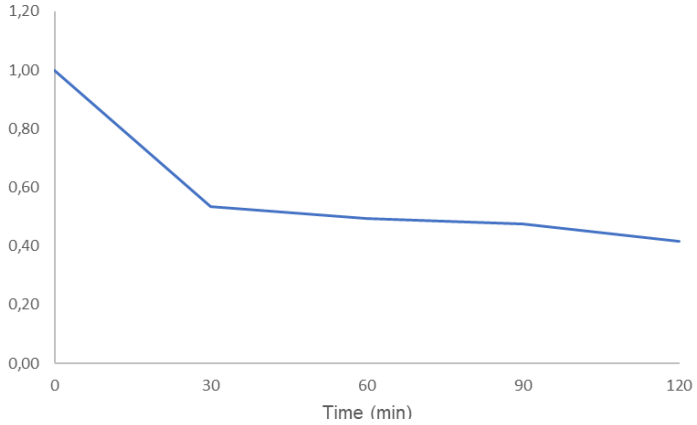

Figure 40 – Residual strength graph: 16 mm Rebar / 98 mm RW.

Table 13 – Bending resistance data: 16 mm Rebar / 98 mm RW.

Classe Aço	280 MPa			320 MPa			Variation of the Resistance during fire (average)
Concrete Height [mm] / Time [min]	60	90	120	60	90	120	
0	1,00	1,00	1,00	1,00	1,00	1,00	1,00
30	0,53	0,55	0,54	0,51	0,53	0,54	0,53
60	0,49	0,51	0,51	0,47	0,49	0,50	0,49
90	0,47	0,49	0,48	0,45	0,47	0,48	0,47
120	0,44	0,42	0,41	0,42	0,40	0,41	0,42

Figure 41 presents data for the configuration with 12 [mm] rebar and 130 [mm] of rockwool. The increased thickness of the rockwool noticeably improves the preservation of the bending moment over time by reducing the rate of thermal degradation compared to previous configurations. Although the initial loss of strength during the first 30 minutes remains significant, it is slightly reduced, suggesting that the thicker insulation delays the heating of the structure. The influence of concrete thickness remains apparent, with thicker slabs demonstrating better structural performance.

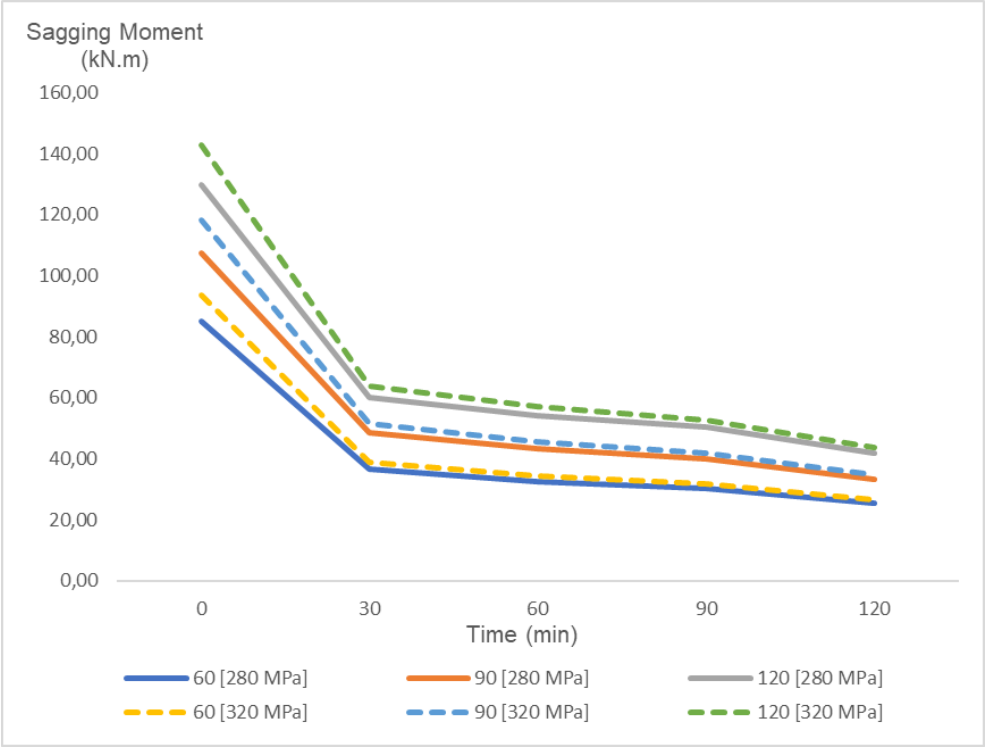

Figure 41 – Sagging Moment Evolution Under Fire: 12 mm Rebar / 130 mm RW.

At the end of 120 minutes, the average reduction in the load-bearing capacity remains close to 30% of the initial strength, similar to the behaviour observed in earlier stages, but with a slight advantage over configurations with thinner insulation, as detailed in Figure 42 and Table 14. This reinforces the importance of efficient thermal insulation in preserving the structural capacity of the slab during prolonged fire exposure. However, despite this improvement, thermal degradation continues, suggesting that a combination of enhanced insulation and appropriate structural reinforcement remains essential to optimise the slab's performance under high temperatures.

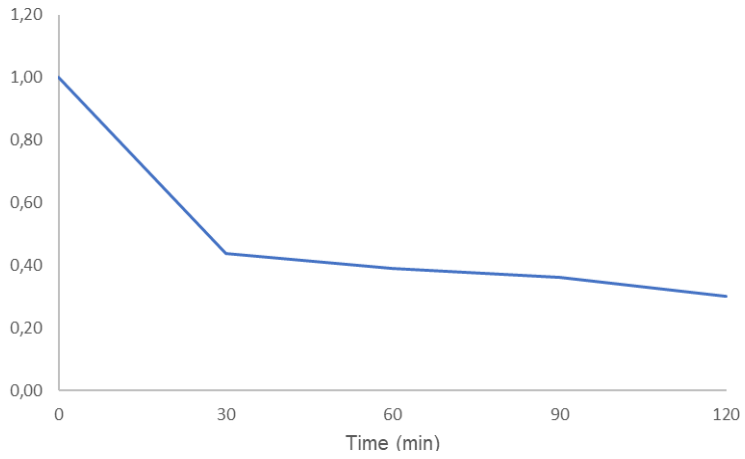

Figure 42 – Residual strength graph: 12 mm Rebar / 130 mm RW.

Table 14 – Bending resistance data: 12 mm Rebar / 130 mm RW.

Classe Aço	280 MPa			320 MPa			Variation of the Resistance during fire (average)
Concrete Height [mm] / Time [min]	60	90	120	60	90	120	
0	1,00	1,00	1,00	1,00	1,00	1,00	1,00
30	0,43	0,45	0,46	0,41	0,43	0,45	0,44
60	0,38	0,40	0,42	0,37	0,38	0,40	0,39
90	0,36	0,37	0,39	0,34	0,35	0,37	0,36
120	0,30	0,31	0,32	0,28	0,29	0,31	0,30

Finally, Figure 43 presents the results for the configuration with 16 [mm] rebar and 130 [mm] of rock wool. As expected, this configuration combines the best structural strength parameters observed in previous stages, resulting in a lower rate of thermal degradation over time. The initial bending moment is higher due to the larger rebar diameter, and the thicker rockwool provides a more effective delay in the loss of thermal strength, leading to a smoother degradation curve. For this final group of configurations, as indicated by the detailed data in Table 15 and Figure 44, the average residual strength after 120 minutes reaches approximately 39% of the initial strength, a value slightly higher than that of the previous configurations. This trend confirms that the combination of more robust rebar with thicker thermal insulation contributes to better preservation of the slab's structural integrity under high temperatures. Nevertheless, even with this optimized configuration, the loss of strength remains significant, highlighting that for scenarios of prolonged fire exposure, additional protection measures may be necessary to ensure adequate structural performance.

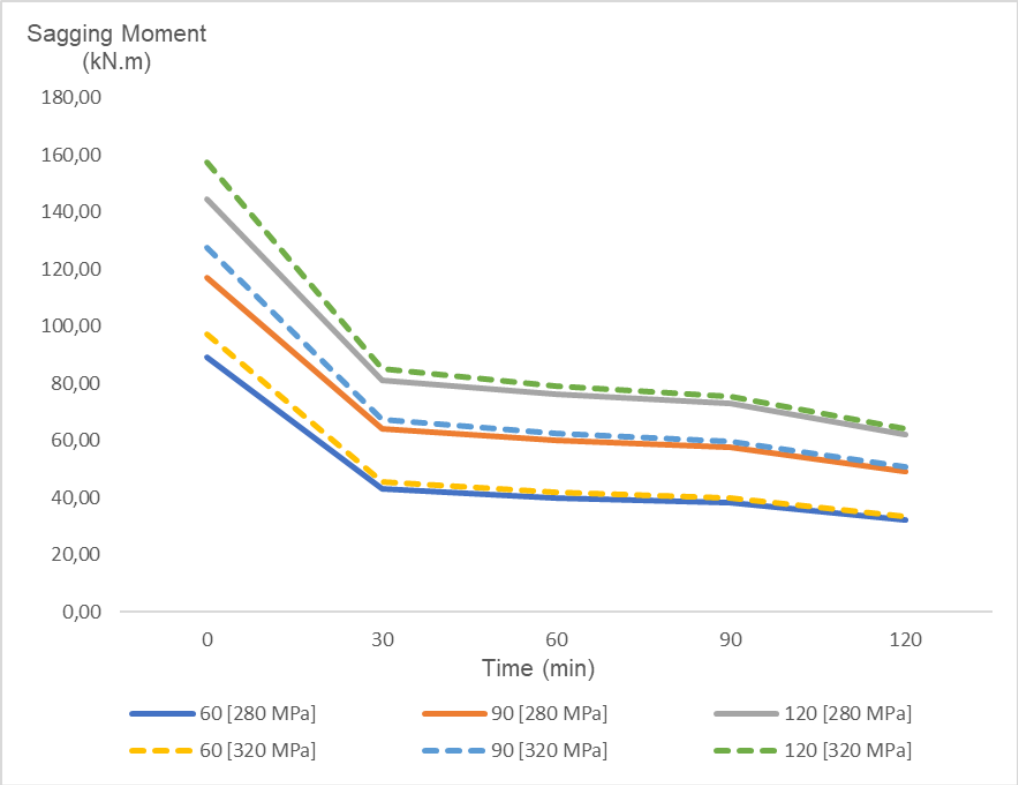

Figure 43 – Sagging Moment Evolution Under Fire: 16 mm Rebar / 130 mm RW.

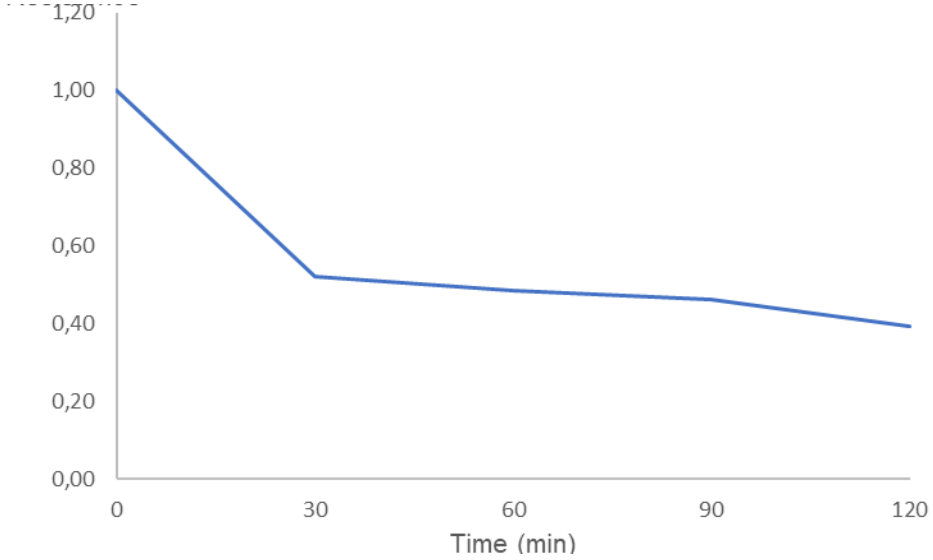

Figure 44 – Residual strength graph: 16 mm Rebar / 130 mm RW.

Table 15 – Bending resistance data: 16 mm Rebar / 130 mm RW.

Classe Aço	280 MPa			320 MPa			Variation of the Resistance during fire (average)
Concrete Height [mm] / Time [min]	60	90	120	60	90	120	
0	1,00	1,00	1,00	1,00	1,00	1,00	1,00
30	0,48	0,55	0,56	0,47	0,53	0,54	0,52
60	0,45	0,51	0,53	0,43	0,49	0,50	0,48
90	0,43	0,49	0,50	0,41	0,47	0,48	0,46
120	0,36	0,42	0,43	0,34	0,40	0,41	0,39

6. NEW PROPOSAL

The assessment of the thermal behaviour of composite slabs under fire conditions is essential for structural analysis, since rising temperatures compromise material properties, reducing load-bearing capacity and increasing the risk of collapse. Currently, there is no standardised regulatory model for determining the temperature distribution in these elements, making laboratory testing the conventional approach—although such tests demand considerable time and financial investment. For this reason, numerical models based on the Finite Element Method (FEM), such as those implemented in ANSYS, have been adopted. While accurate, these models require specialised knowledge and substantial computational resources.

Given these limitations, a simplified calculation model is proposed, based on numerical results obtained in ANSYS. This model enables practical estimation of the temperature at different points within the slab during fire exposure. It is not intended to replace detailed numerical analyses, but rather to offer an alternative tool for engineers to quickly verify whether a slab meets the 120-minute fire resistance requirement, as mandated by the Eurocode. This approach allows for forecasting the thermal evolution over time and can be directly applied in the design phase for evaluating structural safety under fire conditions. Thus, the model contributes effectively to the adoption of more efficient and accessible design solutions for slabs subjected to high temperatures.

The formulation results were derived from ANSYS simulations, and the model's effectiveness was validated through comparison with laboratory experimental data, as detailed in Section 4.4 of this study. This integration of numerical and experimental methods reinforces the reliability and practical applicability of the proposed model.

6.1. Development Framework

The primary objective in developing the calculation model was to derive a mathematical formulation capable of estimating the temperature at various points within the slab. Although the base model studied was the Cofradal 200 slab, the proposed formulation aims to cover a range of configurations, enabling temperature estimation for variations in rock wool thickness and concrete height, as well as for any desired time interval. Accurate temperature prediction is essential for assessing the structural safety of the slab under fire, considering that elevated temperatures directly

affect the mechanical properties of steel and concrete, reducing their strength. Accordingly, the proposed model seeks to provide a simplified tool for thermal estimation, eliminating the need for new complex computational simulations whenever it is necessary to evaluate the slab's temperature under different conditions.

To formulate the model, a set of 18 numerical simulations was carried out in ANSYS, considering various geometric configurations of the slab. Each simulation was evaluated at four different fire exposure durations (30, 60, 90, and 120 minutes). The parametric study considered three rock wool thicknesses (130 mm, 98 mm, and 60 mm), two reinforcement bar diameters (12 mm and 16 mm), and three concrete layer heights (200 mm, 230 mm, and 260 mm). By combining these variables and analysing the results across the four exposure times, data were extracted to support the formulation of the mathematical model, ensuring that the resulting equations could encompass a wide range of structural conditions.

The definition of analysis points within the slab was a key factor in the model's formulation. Since the thermal distribution across the slab section is not homogeneous, five strategic points were selected for monitoring: lower flange, web 1, web 2, upper flange, and rebar. These locations were chosen for their relevance to the structure's thermal response and their influence on slab performance under fire. For each point, an independent formulation was developed, ensuring that the fitted equations accurately reflect the temperature evolution at each specific location within the slab.

It is important to note that the steel yield stress was not included in either the simulations or the model formulation, as its variation does not influence the temperature at a given point in the slab. While temperature directly affects steel strength, the reverse is not true: altering the yield stress does not affect thermal distribution. For this reason, all analyses focused exclusively on predicting temperatures in the slab components, without incorporating variables related to the mechanical resistance of the materials.

The data extracted from ANSYS simulations were systematically organised to support the definition of a simplified mathematical model. For each point in the slab, temperature variation patterns were identified as functions of fire exposure time and the analysed geometric properties. Based on these patterns, the equations were calibrated so that the estimated temperatures closely matched the numerical values. Thus, the developed model allows for quick estimation of temperature at any of the

analysed points, based on the slab's geometric characteristics and fire exposure time, without requiring new simulations.

6.2. Mathematical Formulation

Based on the results obtained from the numerical simulations carried out in ANSYS, a simplified mathematical model was developed to estimate the temperature at different points of the slab over time during fire exposure. The model was structured using a linear equation, calibrated separately for each of the five analysed points in the slab: lower flange, web 1, web 2, upper flange, and rebar, as illustrated in Figure 2. The general equation adopted is given by:

$$\theta = b_0 + b_1 \cdot H_c + b_2 \cdot H_{lr} + b_3 \cdot t \tag{17}$$

Where:

- θ = Estimated temperature at the analysed point (°C);
- b_0 = Intercept coefficient;
- b_1 = Coefficient associated with the height (in mm) of the concrete layer (H_c);
- b_2 = Coefficient associated with the height (in mm) of the rockwool layer (H_{lr});
- b_3 = Coefficient associated with the duration (in minutes) of fire exposure (t).

Each analysed point in the slab exhibited distinct thermal behaviour over time, requiring specific equations to represent the temperature evolution at each location. The coefficients b_0, b_1, b_2 and b_3 were individually adjusted based on the simulation results, ensuring that the formulated equations accurately reflected the observed patterns.

It is worth noting that, although the inclusion of the reinforcement bar diameter as an additional variable (coefficient, b_4) was initially considered, the results showed that this parameter did not significantly influence the temperature estimation. In practical terms, incorporating b_4 did not notably reduce the Root Mean Square Error (RMSE), and in some cases, such as in the Web 2 region, it even led to a substantial increase in error, indicating a decrease in the model's accuracy. Moreover, the thermal effect on the rebar is largely mitigated by the surrounding concrete layer, whose thickness is already accounted for in the model via the variable H_c. Therefore, only the

variables related to the geometry of the thermal protection system (concrete and rock wool) and the fire exposure duration were retained, ensuring a more streamlined, robust, and practical model.

The Lower Flange region, located at the bottom of the steel beam and directly exposed to fire, exhibited the fastest heating rate – a predictable thermal behaviour, given the minimal influence of the rock wool and concrete layers. The graph in Figure 45 shows the comparison between the values obtained from ANSYS and the newly adjusted equation for this region (Equation 18). The RMSE for this comparison was calculated as 16.87 [°C], which falls within acceptable limits, as discussed in Chapter 4.1.

$$\theta = 757{,}37 + 0{,}0 \cdot H_c + 0{,}10 \cdot H_{lr} + 2{,}36 \cdot t \tag{18}$$

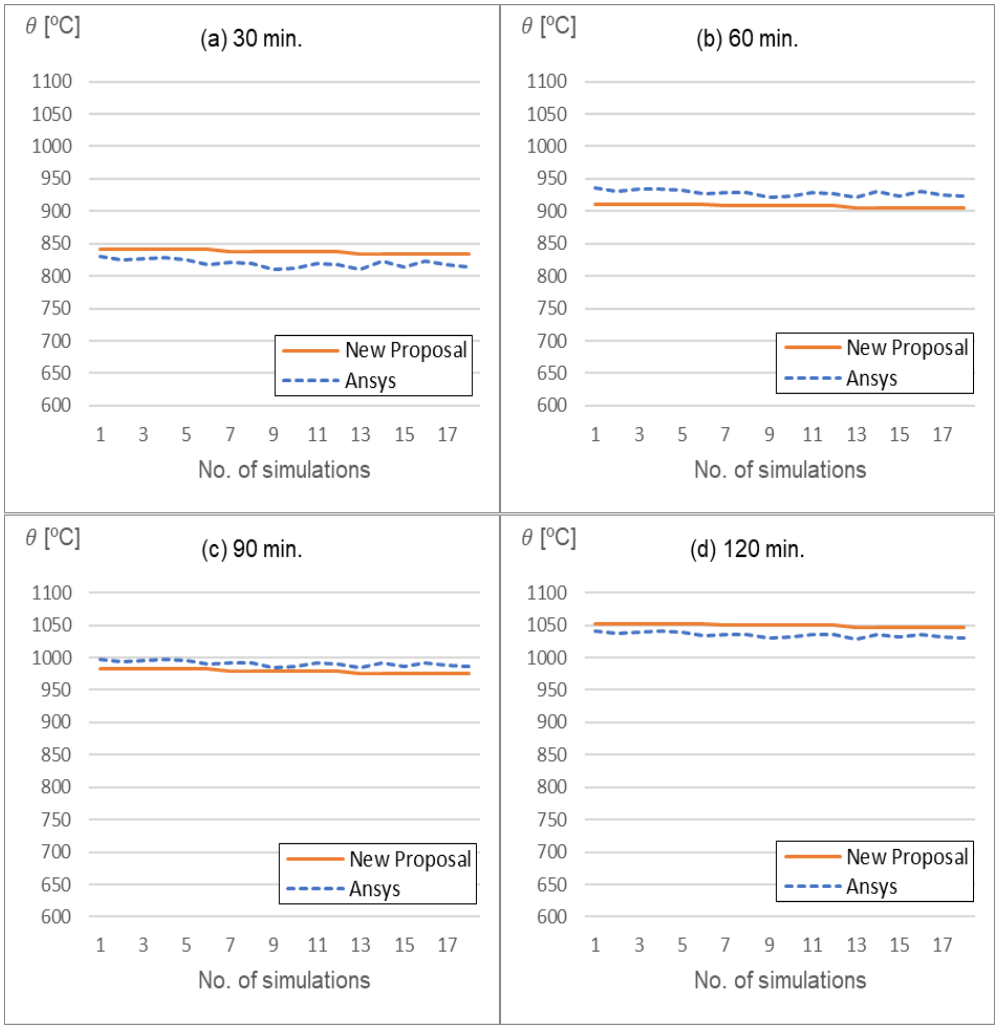

Figure 45 – Model Validation: ANSYS and Eq. 18.

The Web 1 region, located in the first layer of the beam's web, is a transition area with complex thermal conduction behaviour. This region receives heat by conduction from the Lower Flange while simultaneously dissipating heat toward the upper structure. The new model successfully captured the thermal evolution in Web 1. The adjusted equation is presented as Equation 19, with an RMSE of 24.99 [°C] – representing a good fit for this more dynamic region in terms of heat dissipation. Figure 46 illustrates the comparison of graphs for all simulations performed.

$$\theta = 629{,}17 + 0{,}02 \cdot H_c + 0{,}22 \cdot H_{lr} + 2{,}96 \cdot t \tag{19}$$

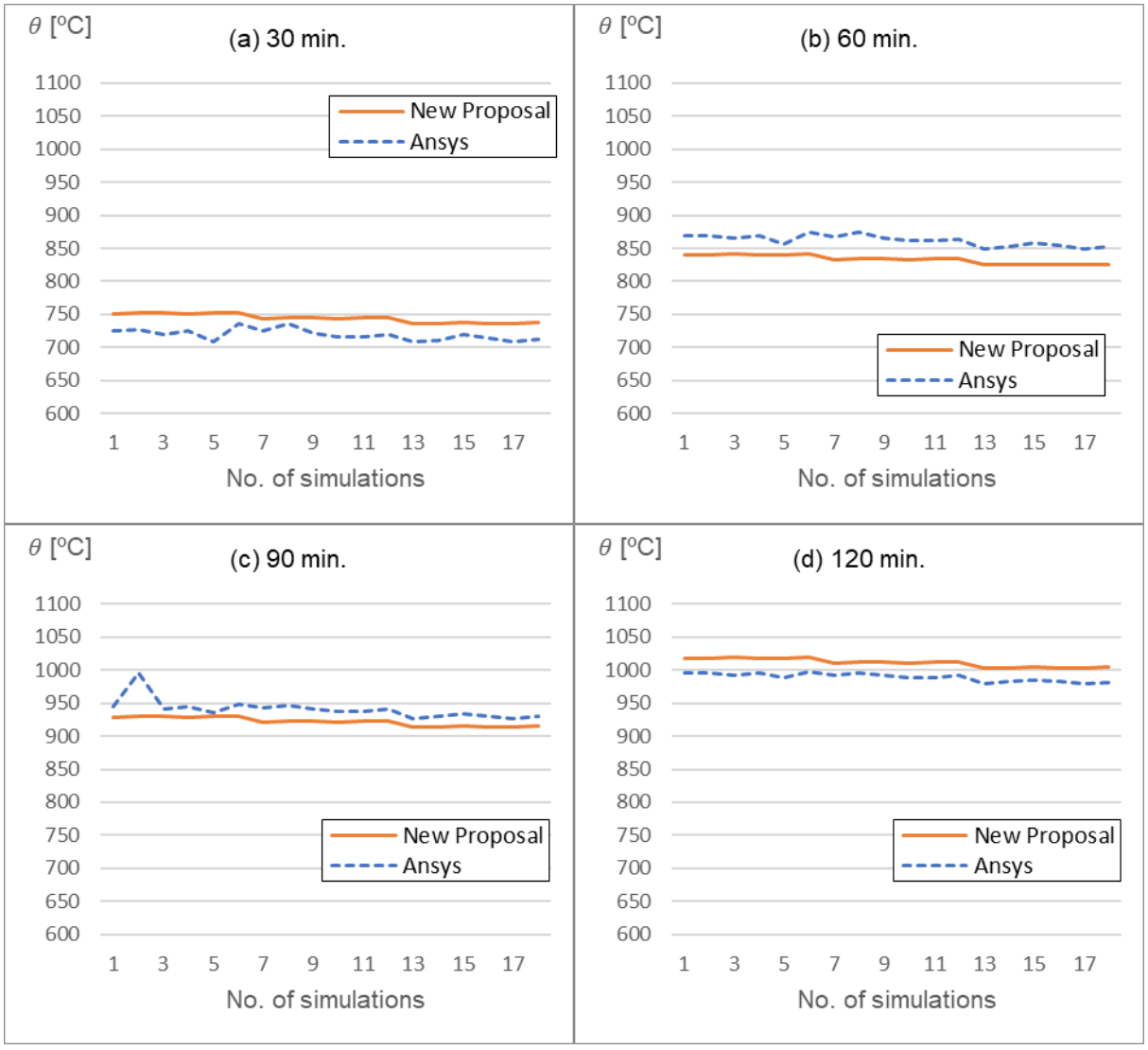

Figure 46 – Model Validation – ANSYS and Eq. 19.

The Web 2 region, being farther from the direct heat source, exhibited lower temperatures than Web 1 but still responded significantly to fire exposure. Equation 20 accurately predicted the thermal variation in Web 2, with an RMSE of 22.03 [°C]. The result, also depicted in Figure 47, reinforces the importance of thermal conduction in the heat propagation across the slab's cross-section.

$$\theta = 159{,}43 + 0{,}12 \cdot H_c + 0{,}35 \cdot H_{lr} + 3{,}15 \cdot t \tag{20}$$

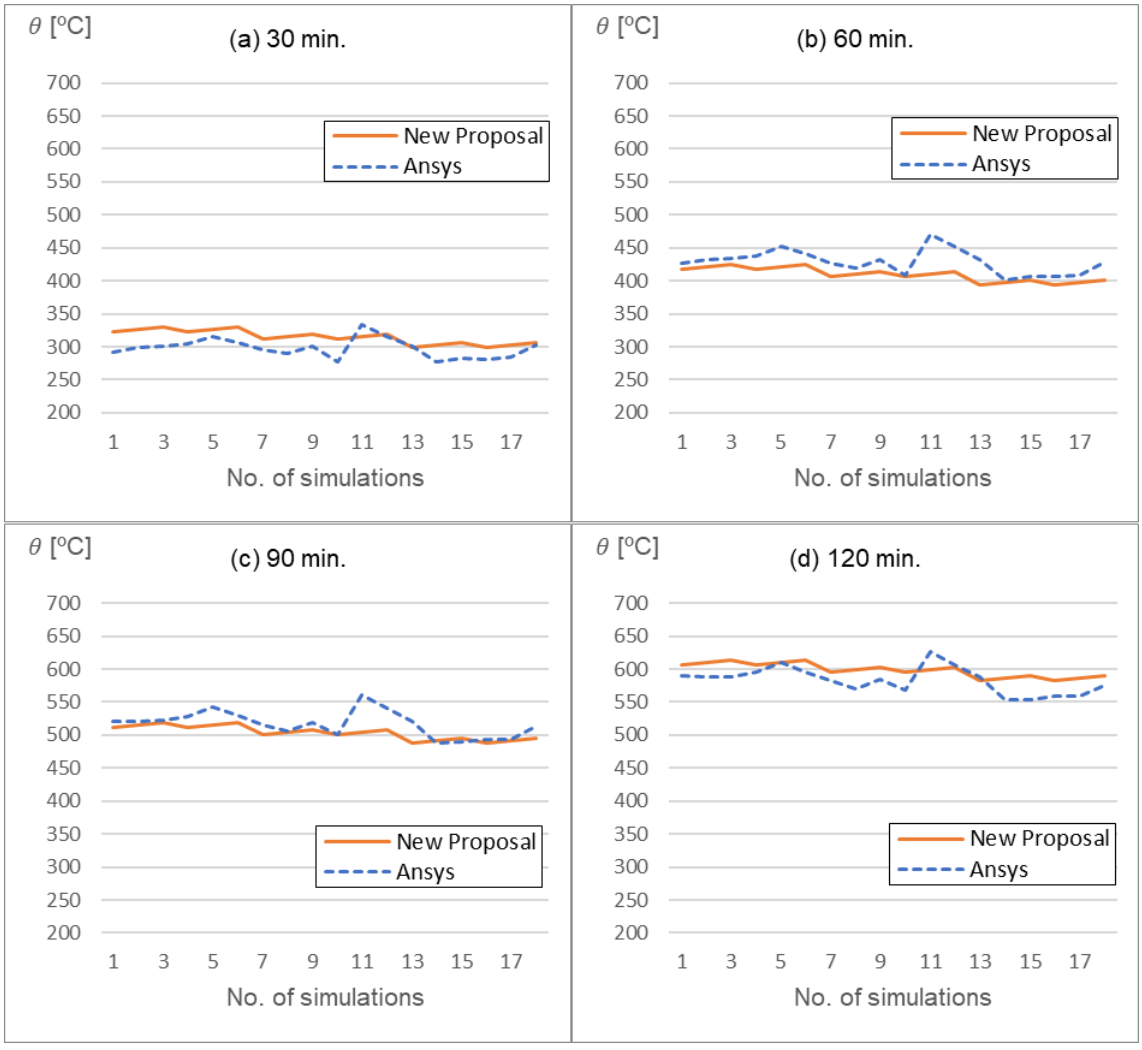

Figure 47 – Model Validation – ANSYS and Eq. 20.

The Upper Flange, located at the top of the steel beam and in direct contact with the concrete, showed the most thermally stable behaviour among all analysed sections. Due to the protection offered by the concrete, the temperature variation over

time was smoother. The proposed model, represented by Equation 21, showed an excellent correlation with the ANSYS values, resulting in a low RMSE of 6.59 [°C]. Figure 48 demonstrates this stability, confirming that the linear equation accurately captured the thermal behaviour of this region.

$$\theta = 0{,}00 + 0{,}00 \cdot H_c + 0{,}22 \cdot H_{lr} + 2{,}29 \cdot t \tag{21}$$

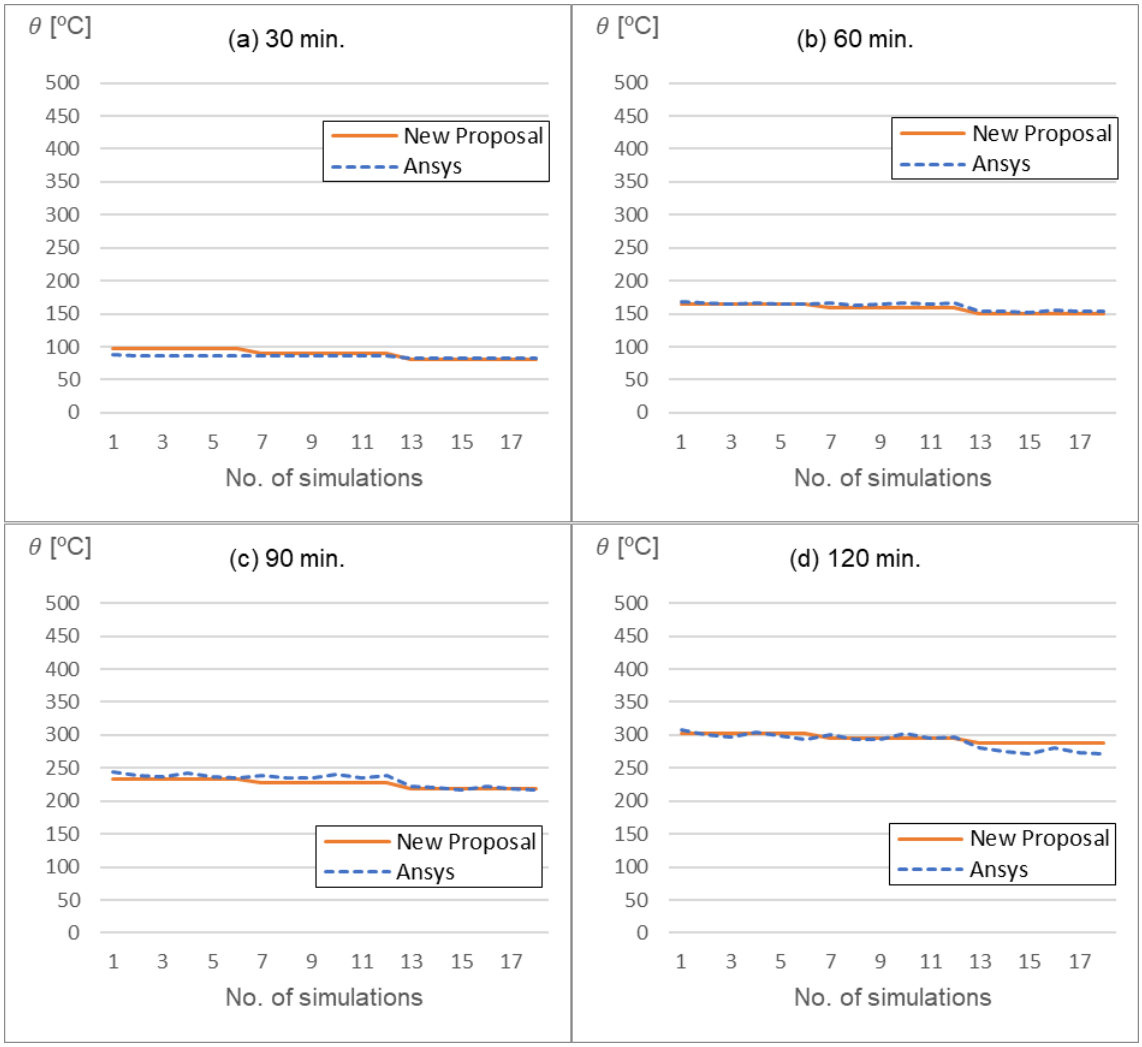

Figure 48 – Model Validation – ANSYS and Eq. 21.

The Reinforcement Bar (Rebar) embedded within the concrete has its temperature directly influenced by the protective capacity of the surrounding materials. The new model adjusted for this region, as expressed in Equation 22, shows that the time-related coefficient indicates a more pronounced heating trend over fire exposure,

while the presence of rock wool plays a crucial role in mitigating this increase. The RMSE of 16.52 [°C] and Figure 49 confirm the model's ability to faithfully represent the thermal behaviour of the reinforcement.

$$\theta = 7{,}44 + 0{,}01 \cdot H_c + 0{,}57 \cdot H_{lr} + 3{,}38 \cdot t \tag{22}$$

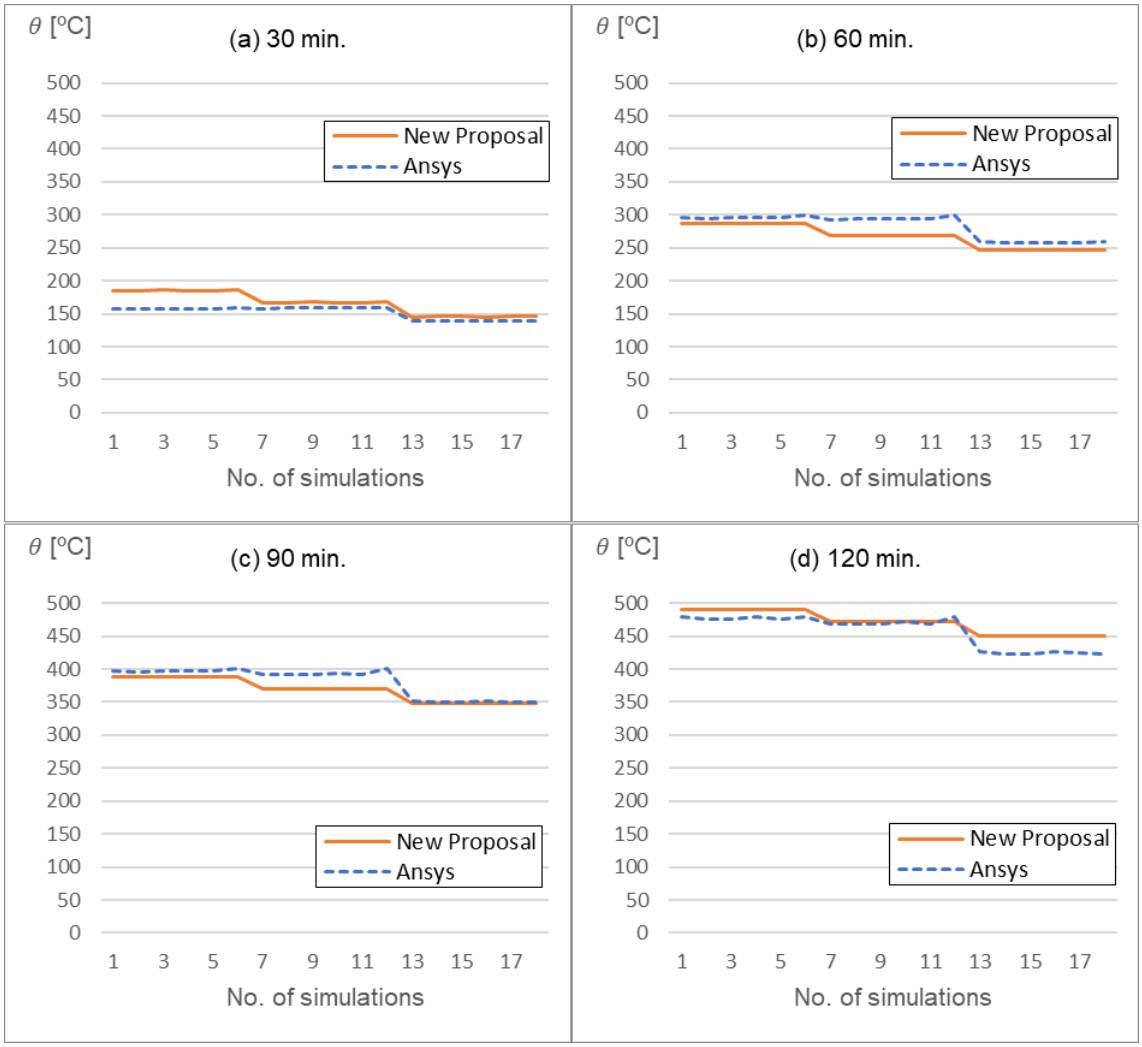

Figure 49 – Model Validation – ANSYS and Eq. 22.

The adjusted coefficients, along with the Root Mean Square Error (RMSE) values, are summarized in Table 16 below. These values highlight the performance of the model for each analysed point of the composite slab under fire conditions.

Table 16 – Adjusted coefficients and RMSE for each point of the slab.

	b0	b1	b2	b3	RMSE
LOWER FLANGE	757,37	0,00	0,10	2,36	16,87
WEB 1	629,16	0,02	0,22	2,96	24,99
WEB 2	159,44	0,12	0,35	3,15	22,03
UPPER FLANGE	1,00	0,00	0,21	2,29	6,59
REBAR	10,08	0,01	0,45	3,37	16,52

The analysis of the results shows that the Lower Flange and Rebar regions exhibited excellent agreement between the values estimated by the model and those obtained from the ANSYS numerical simulations. The Upper Flange, in turn, stood out with the lowest absolute error value, being the most accurately represented region in the model.

The Web 1 and Web 2 regions, which exhibit more complex thermal behaviour due to heat dissipation in transition zones, presented slightly higher error values. Nevertheless, the RMSE values remained within an acceptable range, demonstrating that the model is robust even under conditions of greater thermal variability.

Based on these results, it can be affirmed that the developed model constitutes a practical, reliable, and efficient tool for estimating the thermal evolution of composite slabs under fire exposure. Its simplicity and accuracy make it suitable for applications in structural design and verification, eliminating the need for complex computational simulations during early design phases. Moreover, the model can be easily incorporated into code-based verifications, contributing to faster and more accessible analyses within the context of fire safety engineering.

7. CONCLUSIONS AND FUTURE WORKS

7.1. Conclusions

The investigation of the impact of temperature on the sagging moment of composite slabs with steel deck is highly relevant in the context of structural design under fire conditions, especially given the current limitations of technical standards regarding detailed thermal modelling of such systems. The behaviour of composite slabs under high temperatures involves complex interactions between their components – concrete, structural steel, and insulating materials – which must be well understood to ensure structural integrity and safety.

This study developed a computational model validated against experimental data, which demonstrated excellent agreement with laboratory results. This validation was essential to ensure the reliability of the numerical simulations and, more importantly, to support the development of a simplified thermal modelling approach. The proposed formulation proved effective in predicting the temperatures at various points of the composite slab, with good accuracy and consistent behaviour over time during fire exposure.

With the presented equation, it becomes possible to evaluate the thermal behaviour of the individual components of the composite slab, such as the lower and upper flanges of the steel profile, the reinforcement, and the concrete. This level of detail, rarely achievable in conventional analyses, represents a significant advancement in the understanding of the thermal performance of these structures.

Moreover, the proposed formula makes thermal analysis more accessible and efficient in the design of composite slabs, especially considering that the main international codes (such as Eurocode 4) do not provide direct equations for calculating the temperature of individual structural components. Therefore, the proposed tool contributes directly to improving structural design practices in fire situations, both in terms of precision and applicability.

Among the models studied, the best thermal performance was observed in the configuration with 16 mm rebar and 130 mm of rock wool, which retained 39% of residual resistance after fire exposure. Conversely, the model with 12 mm rebar and 60 mm of rock wool exhibited the lowest performance, maintaining only 30% of residual resistance. This comparison highlights the significant influence of reinforcement diameter and insulation thickness on the fire resistance of composite slabs.

Finally, future studies are recommended to apply the developed methodology to other composite slab models, particularly those with geometries different from the one studied in this work. Investigating new types of profiles, infill thicknesses, and insulating materials may further enrich the understanding of the thermal behaviour of these structures and support their safe and rational application in modern engineering.

7.2. Future Works

Several directions can be explored in future research to broaden the scope of this dissertation and enhance the reliability of the proposed equation:

i. Conduct complementary experimental studies using full-scale composite slab prototypes subjected to controlled fire conditions. This approach would allow for validation of the proposed equation under practical scenarios, as well as provide additional data to refine the coefficients and clearly define its range of applicability.

ii. Investigate the influence of different insulating materials on the thermal performance of composite slabs, replacing mineral wool with alternatives such as glass wool, expanded vermiculite, or intumescent foams. This analysis would help assess the adaptability of the proposed formula to other thermal protection systems used in fire engineering.

iii. Integrate the developed thermal equation into complete structural models, directly linking the temperature prediction to the degradation of mechanical properties of the constituent materials. Such integration could enable more accurate estimations of residual bending moment over fire exposure time, contributing to more realistic assessments of structural safety.

- **REFERENCES**

American Society for Testing and Materials. (1918). *ASTM E119: Standard methods of fire tests of building construction and materials*. ASTM.

Atkins, P., & de Paula, J. (2009). *Physical chemistry* (9th ed.). W. H. Freeman.

Behaviour of a multi-storey steel framed building subjected to fire attack. *Journal of Constructional Steel Research*, 46(1–3), 295–295. https://doi.org/10.1016/S0143-974X(98)00122-9

Bolina, F., Tutikian, B., & Rodrigues, J. P. C. (2021). Thermal analysis of steel decking concrete slabs in case of fire. *Fire Safety Journal, 121*, 103295. https://doi.org/10.1016/j.firesaf.2021.103295

Both, C., Fellinger, J. H., & Twilt, L. (1997). Shallow floor construction with deep composite deck: From fire tests to simple calculation rules. *Heron, 42*, 145–158.

British Standards Institution. (1932). *BS 476: Fire-resistance, incombustibility and non-inflammability of building materials and structures*. BSI.

Buchanan, A. H. (2001). *Structural design for fire safety*. Wiley-Blackwell

CEN. (2002). *EN 1991-1-2: Eurocode 1 – Actions on Structures – Part 1-2: Actions on Structures Exposed to Fire*. CEN.

CEN. (2004). EN 1992-1-2: Eurocode 2 – Design of concrete structures – Part 1-2: General rules – Structural fire design. European Committee for Standardization.

CEN. (2004). *EN 1994-1-2: Design of composite steel and concrete structures — Part 1-2: General rules — Structural fire design* (Annex D). CEN.

CEN. (2004). EN 1995-1-2: Eurocode 5 – Design of timber structures – Part 1-2: General – Structural fire design. European Committee for Standardization.

CEN. (2005). *EN 1993-1-2: Eurocode 3 – Design of Steel Structures – Part 1-2: General Rules – Structural Fire Design*. CEN.

CEN. (2005). *EN 1994-1-2: Eurocode 4 – Design of Composite Steel and Concrete Structures – Part 1-2: General Rules – Structural Fire Design*. CEN.

CEN. (2020). *EN 1363-1: Fire resistance tests — Part 1: General requirements*. European Committee for Standardization.

CEN. (2021). *prEN 1992-1-2: Eurocode 2 – Design of concrete structures – Part 1-2: General rules – Structural fire design* [Draft version]. European Committee for Standardization.

Çengel, Y. A., & Boles, M. A. (2006). *Termodinâmica* (5ª ed.). McGraw-Hill: São Paulo.

Çengel, Y. A., & Ghajar, A. J. (2006). *Heat and mass transfer: Fundamentals and applications* (3rd ed.). McGraw-Hill.

Coelho, N. A., Rêgo, J. H. S., & Pedroso, L. J. (2014). Comparação de resultados analíticos para a equação do calor com o ANSYS.

Cooke, G. M. E., Lawson, R. M., & Newman, G. M. (1988). *Fire resistance of composite deck slabs*.

Costa, C. N., & Silva, V. P. (2006). Revisão histórica das curvas padronizadas de incêndio. In *Seminário Internacional NUTAU* (p. 13). São Paulo.

del Coz-Díaz, J. J., Martínez-Martínez, J. E., Alonso-Martínez, M., & Álvarez Rabanal, F. P. (2020). Comparative study of lightweight and normal concrete composite slabs behaviour under fire conditions. *Engineering Structures, 207*, 110196. https://doi.org/10.1016/j.engstruct.2020.110196

Duponchel, X. (2006). *Etude du comportement au feu du plancher cofradal 200* (Report No. 26004514) [Technical report]. Centre Scientifique et Technique du Bâtiment (CSTB). France.

Duponchel, X. (2011). *Etude du comportement au feu des planchers cofradal STD 200, 230 et 260 et renforce R230* (Report No. 26031330) [Technical report]. Centre Scientifique et Technique du Bâtiment (CSTB). France.

European Convention for Constructional Steelwork, Technical Committee 3. (1984). *Calculation of the fire resistance of composite concrete slabs with profiled steel sheet exposed to the standard fire* (No. 32-37). European Convention for Constructional Steelwork.

European Convention for Constructional Steelwork. (1984). *Fire design of composite steel and concrete slabs* (Publication No. 32). Brussels, Belgium: ECCS.

Franssen, J.-M., & Vila Real, P. (2010). *Fire design of steel structures* (1st ed.). ECCS – European Convention for Constructional Steelwork: Berlin.

Friedman, C., & Lemerle, C. (2001, outubro). *Relatório de ensaio nº RS01-156 relativo à resistência ao fogo de um elemento de construção*.

Gillie, M., Usmani, A., & Rotter, J. (2002). A structural analysis of the Cardington British steel corner test. *Journal of Constructional Steel Research, 58*(4), 427–442. https://doi.org/10.1016/S0143-974X(01)00066-9

Guo, S. (2012). Experimental and numerical study on restrained composite slab during heating and cooling. *Journal of Constructional Steel Research, 69*(1), 95–105. https://doi.org/10.1016/j.jcsr.2011.08.009

Guo, S., & Bailey, C. (2011). Experimental behaviour of composite slabs during the heating and cooling fire stages. *Engineering Structures, 33*(2), 563–571. https://doi.org/10.1016/j.engstruct.2010.11.014

Hamerlinck, A. F. (1991). *The behaviour of fire-exposed composite steel/concrete slabs* (Tese de doutorado, Technische Universiteit Eindhoven). Eindhoven, Países Baixos.

Hamerlinck, R., & Stark, J. W. B. (1990). A numerical model for fire-exposed composite steel/concrete slabs. In *Proceedings of the 10th International Specialty Conference on Cold-Formed Steel Structures* (pp. 115–130).

International Organization for Standardization. (1975). *ISO 834: Fire-resistance tests — Elements of building construction*. ISO.

International Organization for Standardization. (1999). *ISO 834-1: Fire resistance tests — Elements of building construction — Part 1: General requirements* (Standard). International Organization for Standardization. Geneva, Switzerland

K. Jacquemet; C. Lemerle - "Relatório de ensaio nº RS02-092 relativo à resistência ao fogo de um elemento de construção" – 05/2003.

Kamal, M. M., & Ghali, A. (2018). *Effect of elevated temperature on the properties of concrete: A review.* Construction and Building Materials, 186, 256–271.

Kodur, V. K. R., & Dwaikat, M. (2008). A numerical model for predicting the fire resistance of reinforced concrete beams. *Cement & Concrete Composites*, *30*(5), 431–443.

Kodur, V., & Agarwal, P. (2014). Effect of elevated temperature on concrete and steel: A review. *Fire Technology, 50*(3), 585–624.

Lamont, S., Usmani, A., & Drysdale, D. (2001). Heat transfer analysis of the composite slab in the Cardington frame fire tests. *Fire Safety Journal*, *36*, 815–839.

Lienhard, J. H., IV, & Lienhard, J. H., V. (2017). *A heat transfer textbook* (p. 757). Phlogiston Press: Massachusetts.

Lim, L. C. S., & Wade, C. A. (2002). *Experimental fire tests of two-way concrete slabs* (Fire Engineering Research Report 02/12). University of Canterbury and BRANZ Ltd.

Lim, L., Buchanan, A., Moss, P., & Franssen, J.-M. (2004). Numerical modelling of two-way reinforced concrete slabs in fire. *Engineering Structures, 26*, 1081–1091.

Martins, M. (2000). *Dimensionamento de estruturas de aço em situação de incêndio* [Dissertação de mestrado, Universidade Federal de Minas Gerais]. Programa de Pós-Graduação em Engenharia de Estruturas. https://pos.dees.ufmg.br/defesas/74M.PDF

Ministry of Internal Affairs, Decree No. 1532/2008, Technical regulation of fire safety in buildings, December 29, 2008.

Oliveira, T. A. C. P. de. (2018). *Resistência mecânica residual de vigas em concreto armado após o incêndio – análise numérica* [Dissertação de mestrado, Universidade Federal de Pernambuco].

Piloto, P. A. G., [outros autores], & et al. (2020). Effect of the load level on the resistance of composite slabs with steel decking under fire conditions. *Journal of Fire Sciences, 38*(2), 212–231.

Piloto, P., [outros autores], & et al. (2019, August). Three-dimensional numerical modelling of fire-exposed composite slabs with steel deck. *MATTER: International Journal of Science and Technology, 5*, 48–67.

Piloto, P., Prates, L., Balsa, C., & Rigobello, R. (2018, April). Numerical simulation of the fire resistance of composite slabs with steel deck. *International Journal of Engineering and Technology (UAE), 7*, 83–86.

Piloto, P., Prates, L., Balsa, C., & Rigobello, R. (2019). Fire resistance of composite slabs with steel deck: From experiments to numerical simulation. *Portuguese Association for Experimental Mechanics, 31*, 85–94.

Rigobello, R. (2007). *Numerical analysis of steel and composite steel-concrete cross sections and structural elements in fire situation* [Análise numérica de seções transversais e elementos estruturais de aço e aço-betão compostos em situação de incêndio] [Tese de doutorado, University of São Paulo].

Rigobello, R. (2011). *Estruturas de aço aporticadas em situação de incêndio* (Tese de doutorado, Universidade de São Paulo). São Carlos.

Schneider, U. (1982). *Behaviour of concrete at high temperatures* (RILEM Technical Committee 44-PHT). RILEM.

Standards Australia. (1994). *AS 1530.1: Methods for fire tests on building materials, components and structures — Part 1: Combustibility test for materials*. Standards Australia.

Steel, B. (1999). *The behaviour of multi-storey steel framed buildings in fire*. British Steel.

Twilt, L., Hass, R., Klingsch, W., Edwards, M., & Dutta, D. (1994). *Design guide for structural hollow section columns exposed to fire*. Comité International pour le Développement et l'Étude de la Construction Tubulaire: Köln.

Wald, F., et al. (2006). Experimental behavior of a steel structure under natural fire. *Fire Safety Journal, 41*, 509–522.

Wang, Y. C. (2002). *Steel and composite structures: Behaviour and design for fire safety*. London: Spon Press.

Willmott, C. J., & Matsuura, K. (2005). Advantages of the mean absolute error (MAE) over the root mean square error (RMSE) in assessing average model performance. *Climate Research, 30*, 79–82.